

# Asteroid Surface Geophysics

**Naomi Murdoch**

Institut Supérieur de l'Aéronautique et de l'Espace (ISAE-SUPAERO)

**Paul Sánchez**

University of Colorado Boulder

**Stephen R. Schwartz**

University of Nice-Sophia Antipolis, Observatoire de la Côte d'Azur

**Hideaki Miyamoto**

University of Tokyo

The regolith-covered surfaces of asteroids preserve records of geophysical processes that have occurred both at their surfaces and sometimes also in their interiors. As a result of the unique micro-gravity environment that these bodies possess, a complex and varied geophysics has given birth to fascinating features that we are just now beginning to understand. The processes that formed such features were first hypothesised through detailed spacecraft observations and have been further studied using theoretical, numerical and experimental methods that often combine several scientific disciplines. These multiple approaches are now merging towards a further understanding of the geophysical states of the surfaces of asteroids. In this chapter we provide a concise summary of what the scientific community has learned so far about the surfaces of these small planetary bodies and the processes that have shaped them. We also discuss the state of the art in terms of experimental techniques and numerical simulations that are currently being used to investigate regolith processes occurring on small-body surfaces and that are contributing to the interpretation of observations and the design of future space missions.

## 1. INTRODUCTION

Before the first spacecraft encounters with asteroids, many scientists assumed that the smallest asteroids were all monolithic rocks with a bare surface, although, there had been a few articles suggesting possible alternative surface properties and internal structures (e.g., *Dollfus et al.* 1977; *Housen et al.* 1979; *Michel et al.* 2001; *Harris* 2006). Given the low gravitational acceleration on the surface of an asteroid, it was thought that regolith formation would not be possible; even if small fragments of rock were created during the impact process nothing would be retained on the surface (e.g., *Chapman* 1976). However, the NASA Galileo, NEAR-Shoemaker (hereafter simply NEAR) and the JAXA Hayabusa space missions revealed a substantial regolith covering (951) Gaspra, (243) Ida, (433) Eros (*Sullivan et al.* 2002; *Robinson et al.* 2002) and (25143) Itokawa (*Fujiwara et al.* 2006). In addition to finding each of these bodies to be regolith-covered, there is strong evidence that this regolith has very complex and active dynamics. In fact, it was due to the NEAR observations of Eros that the local gravity was first understood to be of importance to asteroid surface processes (*Robinson et al.* 2002). The importance of gravity for regolith dynamics was emphasised even further when the first images were received from the Hayabusa probe.

Over the course of these space missions and others a

wide range of geological features have been observed on the surfaces of asteroids and other small bodies such as the nucleus of comet 103P/Hartley 2 (*Thomas et al.* 2013). However, we do not have direct access to the properties of the granular material that led to these features. Although constitutive equations exist for granular interactions on Earth, the inferred scaling to the gravitational and environmental conditions on other planetary bodies such as asteroids is currently untested. Understanding the dynamics of granular materials in the small-body gravitational environment is vital for the interpretation of their surface geology and is also critical for the design and/or operation of any device planned to interact with their regolith-covered surfaces.

Regolith was originally defined as “a layer of fragmented debris of relatively low cohesion which overlies a more coherent substratum” (*Shoemaker et al.* 1968), although, this definition runs into difficulties when there is no clear interface separating the fragmented debris and the coherent substrate (*Robinson et al.* 2002). Here we will use the term regolith to describe, in general terms, the “loose unconsolidated material that comprises the upper portions of the asteroid” (as defined in *Robinson et al.* 2002). However, we note that self-gravitating aggregates like Itokawa, often referred to as “rubble piles” (*Richardson et al.* 2002), are composed of rubble - boulders of the order of tens of metres and less - held together by gravity and cohesive forces instead of being a monolithic body (*Fujiwara et al.* 2006).

As such they are essentially made of regolith throughout. Therefore, although not discussed in this chapter, understanding how granular materials behave in these extremely low-gravity environments can also improve our understanding of the interiors of these bodies.

This chapter will start by presenting our current knowledge of the surfaces of asteroids (433) Eros, (25143) Itokawa, (21) Lutetia and (4) Vesta. After a short introduction to granular materials, we will then introduce the unique asteroid environment and suggest how this may influence the regolith dynamics. Next, we discuss in detail the underlying physical mechanisms behind the geological processes observed to occur on the surfaces of asteroids. Finally, a discussion of the experimental techniques that can be used to simulate the asteroid environment and the recent advances in modelling regolith dynamics is provided.

## 2. IN-SITU OBSERVATIONS OF ASTEROID SURFACES

In this section we will briefly discuss the in-situ observations of four asteroids: (433) Eros, (25143) Itokawa, (21) Lutetia and (4) Vesta. For more detailed reviews about these bodies the readers are referred to (*Yoshikawa et al.*; *Barucci et al.*; *Russell et al.* (all this volume) and *Cheng 2002*). Additionally, detailed reviews of the geology of other asteroids such as (951) Gaspra, (243) Ida and (253) Mathilde are available elsewhere (e.g., *Carr et al. 1994*; *Sullivan et al. 1996*; *Thomas et al. 1999*).

### 2.1. Asteroid (433) Eros

(433) Eros (hereafter simply Eros; Fig. 1, Table 1), the second largest near-Earth asteroid (NEA), shows a subdued, gently undulating and complex regolith-covered surface, characterised by abundant, but not uniformly distributed, ejecta blocks and conspicuously degraded craters (*Veveřka et al. 2000*; *Veveřka et al. 2001*; *Cheng et al. 1997*). The effective topography on Eros has a range of about 2 km and the slopes, calculated relative to the local gravity vector, vary over the surface of the asteroid (for an explanation of how elevation is defined on irregular bodies see Section 5 of *Cheng et al. 2002a*) with an average slope of  $\sim 8^\circ$  to  $10^\circ$  (*Zuber et al. 2000*; *Thomas et al. 2002*).

**Evidence of regolith motion on Eros** - In general, Eros is very bland in terms of colour and albedo variations. However, visible variations, such as several bright features typically with sharp boundaries, can be seen in regions that have steep slopes (see Fig. 2; *Veveřka et al. 2000*; *Robinson et al. 2001*; *Cheng 2002*; *Mantz et al. 2004*; *Murchie et al. 2002*). As all the NEAR data indicate global compositional homogeneity, the brighter surfaces imply freshly exposed material that has not yet been subjected to space weathering (*Brunetto et al.* (this volume) and *Chapman 2004*). In contrast, dark soils are typically located at the bases of bright streaks and display both diffuse and sharp boundaries (*Thomas et al. 2002*; *Riner et al. 2008*). These ob-

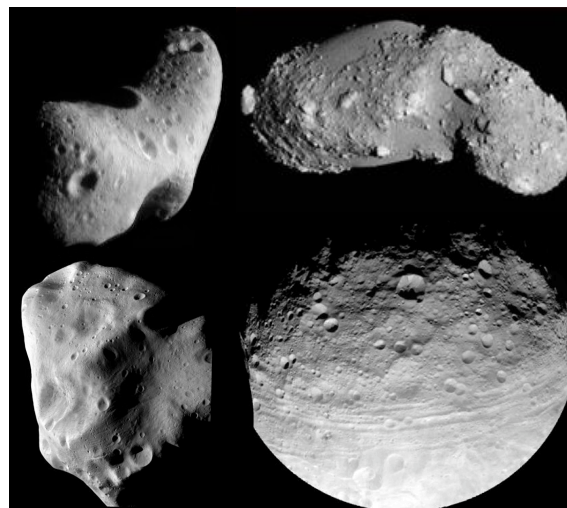


Figure 1: Global images of asteroids (433) Eros (top left), (25143) Itokawa (top right), (21) Lutetia (bottom left) and (4) Vesta (bottom right). Image credits: NEAR/NASA, Hayabusa/JAXA, Rosetta/ESA, Dawn/NASA, respectively.

servations, and morphological data, indicate that the bright streaks are the results of preferential downslope movement or a landslide of mature regolith, revealing immature material beneath (e.g., *Robinson et al. 2002*; *Thomas et al. 2002*; *Riner et al. 2008*; *Murchie et al. 2002*).

Indeed, on closer inspection, accumulations of granular material that have been gravitationally transported away from topographic highs can be seen on Eros (Fig. 2; *Thomas et al. 2002*; *Veveřka et al. 2001*; *Robinson et al. 2002*). These granular deposits appear to result from low momentum downslope movements and some observations suggests that mobilised regolith may even be halted by frictional or other effects before reaching the foot of the slope (*Mantz et al. 2004*; *Thomas et al. 2002*). Downslope motion has also been observed on slopes that are well below the expected angle of repose for granular materials. Whether this indicates the necessity for a triggering mechanism or not is a subject currently under debate (*Cheng 2002*; *Holsapple 2013*).

**Craters and crater morphology on Eros** - Further evidence for regolith motion is that, despite the large number of craters on the surface of Eros, there is a deficiency of small (<2 km diameter) craters (*Veveřka et al. 2000*; *Veveřka et al. 2001*). As there are sufficient projectiles in near-Earth space to produce small craters there must, therefore, be a process that either covers or erodes small craters on Eros (*Veveřka et al. 2001*). It has been suggested that impact-induced seismic shaking (see Section 5), which causes the regolith to move, may erase small crater features and thus explain their paucity compared to predictions of dynamical models of projectile populations (e.g., *Richardson et al. 2004*; *Michel et al. 2009*). However, alternative

degradation mechanisms have also been suggested including micro-cratering and thermal creep (Cheng 2002). See Marchi et al. (this volume) for a detailed discussion of cratering on asteroids.

Additional evidence of resurfacing and modification is visible in the interiors and the subdued rims of several craters (Robinson et al. 2002; Zuber et al. 2000). The depth-to-diameter ratio of craters on Eros is, on average,  $\sim 0.13$ , but the freshest and youngest craters approach lunar values of  $\sim 0.2$  (Robinson et al. 2002). Many of the topographic lows are filled with deposits of fine granular material (Fig. 2 and e.g., Veverka et al. 2001). These features, referred to as “ponds”, are characterised by smooth, level surfaces that are sharply delineated (Robinson et al. 2001; Cheng et al. 2002b). They are found preferentially at low latitudes and in the bottom of small ( $< 1$  km) craters or other topographic lows (Robinson et al. 2001; Cheng et al. 2002b), however, this may be due to observational biases (Roberts et al. 2014b). The bottoms of the ponds are often offset in a direction towards the downslope of the crater (Veverka et al. 2001) and recent results have found that the pond floors are not as flat as originally believed (Roberts et al. 2014a).

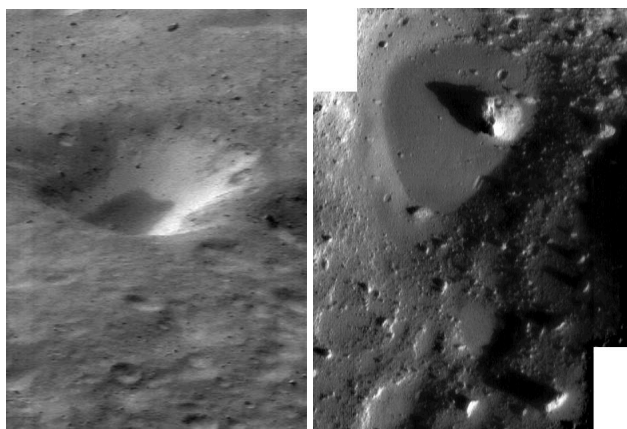


Figure 2: Evidence of regolith transport on Eros - LEFT: Bright, freshly exposed material on a large crater wall, as the darker material moves downslope (PIA03134); RIGHT: An example of a dust pond (2001\_028\_5\_eros.png from <http://ser.sese.asu.edu/near.html>).

**Linear features on Eros -** On the surface of Eros several lineations can be observed including chains of craters, sinuous and linear elongated depressions and topographic ridges (Veverka et al. 2000). Such lineations are similar to those observed on the Martian satellite, Phobos (Thomas et al. 1979). Prockter et al. (2002) explain that, on Eros, these linear features, or grooves, exist on a global scale (prominent wide troughs and ridges several kilometres in length), a regional scale (chains of craters and straight-edged grooves several hundreds of meters long) and also on very local scales (closely spaced ridge and trough terrains tens of meter in scale). The large variations in directions, patterns and

relative ages of the lineations indicate that they were formed during many different and unrelated events (see Section 5 and Marchi et al. (this volume); Veverka et al. 2000; Prockter et al. 2002; Thomas et al. 2002; Robinson et al. 2002). For a full map and analyses of the linear features on Eros see Buczkowski et al. (2008).

**Depth and character of Eros’ regolith -** Eros has a widespread unconsolidated regolith of depths that are typically several tens of meters in thickness, but not uniform over the surface (Cheng 2002; Barnouin-Jha et al. 2001; Veverka et al. 2001; Robinson et al. 2002). The heterogeneity of the regolith depth distribution is probably caused partially by the asymmetric nature of crater ejecta blankets (a consequence of the asteroid’s rotation, see Section 5 and Geissler et al. 1996) and is further accentuated by the irregular spacing of craters and the subsequent downslope motion and regolith transport that, as discussed above, appears to occur commonly on the surface of Eros (Robinson et al. 2002).

The surface of Eros is extremely rough and the surface roughness is approximately self-affine from scales of a few meters to hundred of meters (Cheng 2002). The regolith particles range in size from the fine ( $\ll$ cm - sized) dust particles found in the ponds to the numerous ( $> 10^4$ ) large ( $> 10$  m) ejecta blocks of boulders at the extreme large end of the particle size distribution (Thomas et al. 2002). The morphology of these blocks ranges from angular to fractured to disaggregated (Robinson et al. 2002) and their size distribution is described adequately by a power law with a slope of about -3 on a cumulative plot (Fig. 3). For more information about the nature of these boulders see Marchi et al. (this volume).

## 2.2. Asteroid (25143) Itokawa

Compared to Eros, the NEA (25143) Itokawa (hereafter simply Itokawa; Fig. 1, Table 1) was found, astonishingly, to have entirely different structural and surface properties despite their similar taxonomic class. The reason for these different properties is not clearly understood, but perhaps this shouldn’t have been surprising; because of their size (mass) difference, if gravity is the discriminator, then Itokawa is expected to be as different from Eros, geologically, as Eros is from the Moon (Asphaug 2009).

One of the most remarkable features of Itokawa is the global shape, which seems to consist of two parts: a small “head” and a large “body” separated by a constricted “neck” region (Fig. 1 and Fujiwara et al. 2006; Demura et al. 2006). It is highly likely that Itokawa is a rubble pile asteroid rather than a monolithic body (Fujiwara et al. 2006). The low bulk density of Itokawa (Table 1) provides further evidence for the rubble pile interior structure with estimates suggesting that Itokawa’s macroporosity may be as high as  $\sim 41\%$  (Fujiwara et al. 2006). However, these density measurements do not rule out the presence of a core on the order of 100 m in size.

Table 1: Characteristics of the asteroids discussed in detail in this chapter. <sup>(1)</sup>Cheng et al. (1997); <sup>(2)</sup>Yeomans et al. (2000); <sup>(3)</sup>Miller et al. (2002); <sup>(4)</sup>Veveřka et al. (2000); <sup>(5)</sup>Fujiwara et al. (2006); <sup>(6)</sup>Abe et al. (2006); <sup>(7)</sup>Scheeres et al. (2006); <sup>(8)</sup>Schulz et al. (2012); <sup>(9)</sup>Sierks et al. (2011); <sup>(10)</sup>Lamy et al. (2010); <sup>(11)</sup>Thomas et al. (2012); <sup>(12)</sup>Russell & Raymond (2011); <sup>(13)</sup>Russell et al. (2012)

Asteroid	Space Mission	Mean diameter (km)	Bulk density (g cm <sup>-3</sup> )	Rotation period (h)	Surface acceleration (cm s <sup>-2</sup> )	Escape speed (m s <sup>-1</sup> )
(433) Eros	NASA NEAR <sup>(1)</sup>	~17 <sup>(2)</sup>	2.7 <sup>(2)</sup>	5.3 <sup>(3)</sup>	0.23 - 0.56 <sup>(3)</sup>	~ 1 <sup>(4)</sup>
(25143) Itokawa	JAXA Hayabusa <sup>(5)</sup>	~ 0.32 <sup>(5)</sup>	1.9 <sup>(6)</sup>	12.1 <sup>(7)</sup>	2.4e-3 - 8.6e-3 <sup>(7)</sup>	0.1-0.2 <sup>(5)</sup>
(21) Lutetia	ESA Rosetta <sup>(8)</sup>	~99 <sup>(9)</sup>	3.4 <sup>(9)</sup>	8.2 <sup>(10)</sup>	~5 <sup>(11)</sup>	~70 <sup>(11)</sup>
(4) Vesta	NASA Dawn <sup>(12)</sup>	~526 <sup>(13)</sup>	3.5 <sup>(13)</sup>	5.3 <sup>(13)</sup>	~25	~363

### Depth, character and migration of Itokawa's regolith -

Two different types of terrain - rough and smooth - are observed on Itokawa (Saito et al. 2006). The rough deposits consist of numerous boulders (Fujiwara et al. 2006) and typically exhibit variations in elevation that range from 2-4 m over small lateral distances (Barnouin-Jha et al. 2008). The very highest and roughest parts of the asteroid are covered in large gravel and boulders and are completely devoid of all particles smaller than 1 cm in size (Barnouin-Jha et al. 2008). The smooth terrains - Muses Sea and Sagami-hara - coincide with the low-gravitational potentials and are generally homogeneous, featureless and relatively flat (slopes <8°). This is consistent with a loose granular layer that has been allowed to seek out its minimum energy configuration after the formation of the asteroid (Miyamoto et al. 2007; Fujiwara et al. 2006; Yano et al. 2006; Riner et al. 2008). This idea is further reinforced by the close-up images and measurements taken during the touch down of the Hayabusa spacecraft; these indicate that small regolith particles are being transported into the Muses Sea region and are gradually covering up the boulder-rich surface (Miyamoto et al. 2007; Barnouin-Jha et al. 2008). The regolith depth in the smooth regions on Itokawa is estimated to be approximately 2.5 m (Barnouin-Jha et al. 2008; Cheng et al. 2007).

In general Itokawa's regolith appears to be dominated by grains >1 mm in size (Miyamoto et al. 2007). That said, the regolith particles that were returned to Earth are fine-grained (size range between 3-180 μm, but most < 10 μm; Nakamura et al. 2011). The apparent absence, or at least the small quantity, of fines on the surface of Itokawa may be explained by processes such as electrostatic levitation combined with solar radiation pressure (Lee 1996; Scheeres 2005), segregation of the fines towards the interior of the body (Asphaug 2007; Miyamoto et al. 2007) or simple higher ejection velocities following impacts making reaccumulation difficult (Nakamura et al. 1994). Some of these processes will be discussed later in Sections 4–5.

The size distribution of boulders on Itokawa's surface is estimated to be a power law with a slope of -2.8 to -3.0 on a cumulative plot (Fig. 3). It is possible, however, that the observed distributions on Itokawa may be related

to the preferential displacement of some block sizes relative to others, and the settling locations of differing sized blocks. The abundance of meter-sized boulders (particularly on the western side; Fujiwara et al. 2006), and the fact that decameter-sized boulders exist (the length of the largest boulder is approximately one tenth of the length of Itokawa itself; Saito et al. 2006), indicate that they may have been produced during a catastrophic disruption event, consistent with the rubble pile structure (Fujiwara et al. 2006; Michel et al. 2001).

### Further evidence for an active regolith on Itokawa -

At the boundary of the Muses Sea region with the rough terrain, boulders are typically piled on top of each other without being buried by fines. The larger sized gravels tend to lie over the smaller particles and are aligned with directions coincident with the local gravity slope (Miyamoto et al. 2007). This type of organisation of gravels is referred to as imbrications, in this case with the longest axes of the gravel being preferentially orientated transverse to the granular flow. The positions and orientations of all of the particles indicate that they are stable against local gravity and that the migrations were gravity-induced (Miyamoto et al. 2007).

Evidence of landslide-like deposits can be seen in Fig. 4. There are large boulders that have blocked the migration of smaller particles, resulting in piles of smaller particles on the uphill sides of the boulders (Miyamoto et al. 2007). Unlike the surface of Eros, Itokawa is very heterogenous in colour and albedo, with brighter surfaces being found in three main areas: areas with steeper slopes, areas of local high terrain and apparently eroded areas, e.g., crater rims (Saito et al. 2006). Saito et al. (2006) suggest that this dichotomy is due to dark surfaces being removed, leaving the fresh regolith newly exposed at the surface, as observed on Eros.

All of these observations give a strong indication that regolith on the surface of Itokawa has been relocated since the initial accumulation or deposition.

**Craters and crater morphology on Itokawa -** Itokawa has very few craters in general (the total number of craters on Itokawa is <100 over the entire surface including indef-

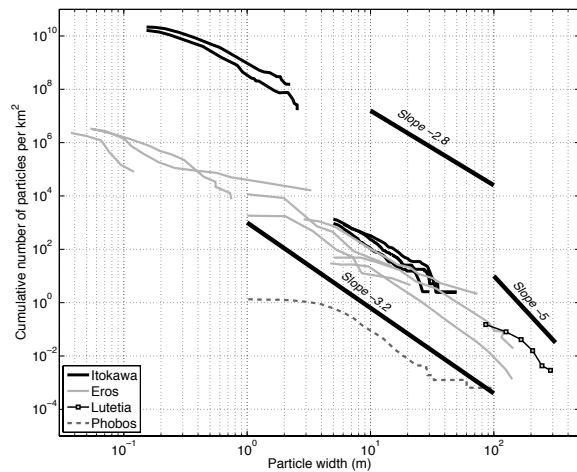


Figure 3: Measured cumulative size distribution as a function of particle size on the surfaces of asteroids and Phobos. Data combined from several papers. Itokawa: *Miyamoto et al. (2007)*, *Saito et al. (2006)*, *Michikami et al. (2008)*, *Mazrouei et al. (2012)*; Eros: *Thomas et al. (2001)*; Lutetia: *Küppers et al. (2012)*; Phobos (a Martian satellite with a mean diameter of  $\sim 22$  km): *Thomas et al. (2002)*. For the papers in which the cumulative number of particles was given, this has been approximately converted to cumulative number per square kilometre using the information provided in the respective papers. A shallower slope may indicate that boulders have experienced less processing, including breaking, sorting and transporting (*Thomas et al. 2002*).

inite candidates) and absolutely no distinct craters  $< 1$  m in diameter (*Saito et al. 2006*; *Fujiwara et al. 2006*). Those craters that do exist on the rough and transitional terrains, and that retain their regolith, are filled with finer particles, similar to the “ponds” seen on Eros. The best example of a crater on the surface of Eros - Komaba - is located near the edge of the highlands. It has a small depth-to-diameter ratio (0.09) consistent with crater formation in a coarse granular target, a flat floor and is surrounded by brighter rims (*Saito et al. 2006*; *Barnouin-Jha et al. 2008*). In addition, there appears, unusually, to be no apparent correlation between the locations of boulders and craters (*Michikami et al. 2008*). These observations are further evidence of regolith motion and suggest that a mechanism is filling in and erasing the craters on the surface of Itokawa. Such a mechanism may well be seismic shaking, as proposed to explain paucity of small craters on Eros (see Section 5). Alternatively, it is also possible that Itokawa could have been generated relatively recently in the main belt before being moved to its current orbit (*Saito et al. 2006*).

**Linear features on Itokawa** - Unlike Eros, there are no global lineaments on Itokawa (*Fujiwara et al. 2006*). How-

ever, on the body of Itokawa subtle local linear features can be observed. These features, caused by the alignment of boulders (*Cheng et al. 2007*), are not as tall as other structures such as large boulders. Nonetheless, they are an important contributor to the topography of Itokawa due to their large lateral extent (*Barnouin-Jha et al. 2008*).

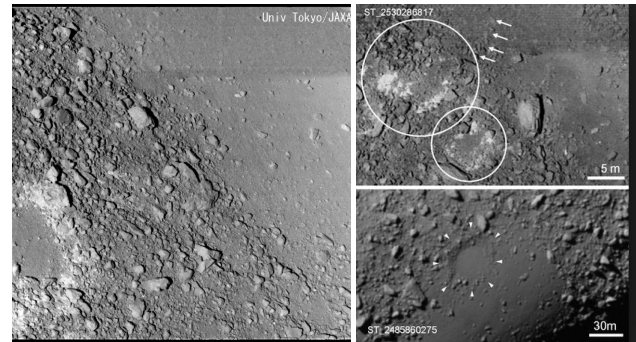


Figure 4: Evidence of regolith transport on Itokawa - LEFT: High resolution image of the boundary area between Muses Sea and the rough terrains. Piles of gravel can be seen on the uphill sides of boulders. Such a characteristic is similar to terrestrial landslide; TOP RIGHT: Image of the Neck area of Itokawa (13cm/pixel) showing piles of angular boulders at the lower part of the image. Crater-like depressions are shown by the circles and the arrows indicate the debris, which appears to have drained from the rim of the upper crater towards the smooth terrain; BOTTOM RIGHT: A circular depression that appears to be filled with finer particles.

### 2.3. Asteroid (21) Lutetia

The main-belt asteroid (21) Lutetia (hereafter simply Lutetia; Fig. 1, Table 1) has a highly complex surface geology with significant interactions between ancient and more recent structures (*Sierks et al. 2011*; *Thomas et al. 2012*).

**Craters and crater morphology on Lutetia** - The higher gravity and escape velocity on Lutetia have provided an environment for continuous ejecta patterns with obvious relations to the impact from which they formed (*Massironi et al. 2012*). The typical depth-to-diameter ratio of craters on Lutetia is 0.12 but values have been observed ranging from 0.05 to 0.3 (*Vincent et al. 2012*). The distribution of depth-to-diameter ratios varies depending on the region of Lutetia’s surface indicating that, not only are there variations of physical properties across the surface, but there are also differences in the surface evolutionary processes (*Vincent et al. 2012*).

*Thomas et al. (2012)* divide the craters on Lutetia into four different categories: standard craters, buried or partially filled craters, distorted or cut craters that have been disturbed by lineament formation, and morphologically non-standard impact structures. By the latter they refer to craters that are not typically bowl-shaped and/or do not

have a round rim and the strange form is not obviously linked to linear features. Such unusually shaped craters (for examples see *Thomas et al. 2012*) could be the result of oblique impacts (*Thomas et al. 2012*; *Herrick & Hessen 2006*; *Krohn et al. 2014*) but other mechanisms have also been proposed (*Vincent et al. 2012*).

Similarly to the surface of Eros, Lutetia's surface exhibits a paucity of small (<1 km) craters. This could perhaps be explained by seismic shaking; however, there is also a depletion in craters of sizes up to 8 km, which is more difficult to attribute to seismic shaking. The craters that have been deformed by linear features are additional evidence that the surface has been modified since the crater formation (*Sierks et al. 2011*).

**Depth and character of Lutetia's regolith -** The surface of Lutetia is covered by an extensive regolith, similar to that of the Moon (*Coradini et al. 2011*). Nonetheless, Lutetia's surface is very heterogeneous. Images taken during the close approach of ESA's Rosetta spacecraft allowed Lutetia's surface to be separated into several distinct regions (for a detailed map of the Lutetia regions see *Sierks et al. 2011*; *Massironi et al. 2012*). Some regions are very old and heavily cratered with significant deformation by linear features, while others exhibit sharp morphological boundaries. The Baetica (North Pole) region contains a cluster of craters, created from a series of superposed impacts (*Massironi et al. 2012*) this is one of the most prominent features imaged on Lutetia's surface. The extremely low crater density and lack of linear features in this region can perhaps be attributed to the covering of smooth regolith material, probably the ejecta blanket from the crater cluster (*Sierks et al. 2011*; *Vincent et al. 2012*).

Lutetia's regolith is estimated to be up to ~600 m in depth (*Vincent et al. 2012*). This estimate is based on the thickness of the ejecta blanket of the largest crater assuming a uniform gravity field and may, therefore, be improved with a more detailed study of regional ejecta geophysics taking into account the complex gravitational field of Lutetia. Surface slopes can exceed 30° in some places but are generally less than this (*Sierks et al. 2011*; *Thomas et al. 2012*). The size distribution of blocks on Lutetia is reported to be a steep power-law of -5 (Fig. 3 and *Küppers et al. 2012*). It is noted, however, that the method used by *Küppers et al. (2012)* for binning the boulders is different to the method used by other research groups.

**Evidence for an active regolith on Lutetia -** Diverse evidence for regolith motion was observed inside the large crater cluster in the North pole (Baetica) region. The observations include albedo variations with bright regions on the steep slopes indicative of relatively recent landslides (as observed inside craters on Eros and on Itokawa), deposits of smooth and fine particles with boulders, and apparent landslide deposits (*Sierks et al. 2011*). In addition, observations show craters that have poorly defined rims as a consequence

of multiple landslides (e.g., Fig. 5 of *Thomas et al. 2012*). Rocky outcrops are also visible at what appears to be the source of the landslides (*Thomas et al. 2012*).

**Linear features on Lutetia -** Lutetia displays a huge number of lineaments (e.g., Fig. 5) that can be found over the entire imaged surface, with the exception of two young regions (*Thomas et al. 2012*). The orientation of these linear features, which are similar in appearance to those on Eros discussed in Section 2.1, has been linked to three impact craters (*Besse et al. 2014*). The linear structures have been classified into several types by *Thomas et al. (2012)*: irregular troughs, large faults and tectonic troughs, organised linear reflectance variations and narrow faults, rows of coalesced pits (known as pit-chains), intra-crater trenches, intra-crater layers and ejecta layers and, finally, scarps and ridges. The most striking linear feature on Lutetia's surface is the very long (~10 km) and wide (~1.2 km maximum width) groove in the Noricum region (*Thomas et al. 2012*). This groove is situated on a local topographic high and is approximately 100 m in depth (*Sierks et al. 2011*). For a very complete discussion of the lineaments on Lutetia, including multiple examples, see *Thomas et al. (2012)*.

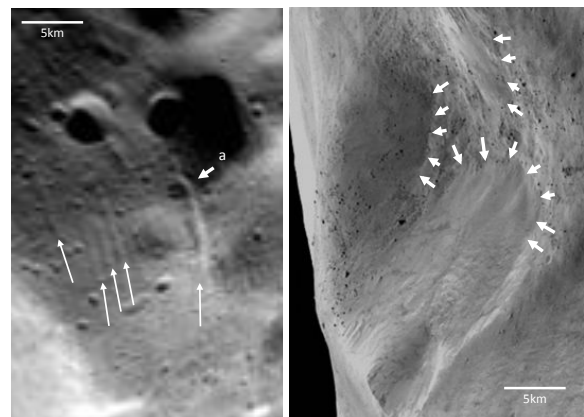


Figure 5: Closeup images of Lutetia - LEFT: Curvilinear features. Some linear features cut crater rims (a) implying these features postdate the craters (ID 224598, ESA 2010 MPS for OSIRIS Team MPS/UPD/LAM/IAA/RSSD/INTA/UPM/DASP/IDA); RIGHT: The central crater cluster in Baetica showing landslides (arrows) and numerous boulders (ID 216820, ESA 2010 MPS for OSIRIS Team MPS/UPD/LAM/IAA/RSSD/INTA/UPM/DASP/IDA)

## 2.4. Asteroid (4) Vesta

(4) Vesta (hereafter simple Vesta; Fig. 1, Table 1) is the second most massive main-belt asteroid and is one of the fastest rotators of the large asteroids. Vesta's surface has a complex topography at all spatial scales (*Jaumann et al. 2012*). One of the most dramatic discoveries on the surface of Vesta is an 18 km high mountain in the centre of

a huge (460 km-wide) crater named the Rheasilvia basin. This peak is the second highest in the Solar System after Olympus Mons on Mars.

**Depth and character of Vesta's regolith -** The thickness of Vesta's regolith is estimated to be approximately 800 m (Jaumann *et al.* 2012). The surface slopes on Vesta can exceed 40° and there are a considerable number of steep slopes that may be indicative of intact bedrock beneath or the presence of cohesive forces in the regolith. Dark materials, of likely exogenic origin (carbon-rich low-speed impactors), are distributed unevenly across Vesta's surface (Fig. 6(a); Jaumann *et al.* 2014).

**Craters and crater morphology on Vesta -** Craters on Vesta display a wide range of degradation states from fresh craters with unmodified rims to impact crater ruins showing almost no visible rims (Jaumann *et al.* 2012). Depth-to-diameter ratios are similar to Lutetia, varying from 0.05 to 0.4 with a mean of 0.17 (Jaumann *et al.* 2012; Vincent *et al.* 2012; Vincent *et al.* 2013). The northern hemisphere is observed to be heavily cratered whereas the southern hemisphere shows comparatively fewer craters, most probably due to the relatively recent basin forming impacts near the south pole (Vincent *et al.* 2013). Shallower craters are found in the oldest regions on the surface of Vesta, as would be expected due to progressive crater degradation. The deep, loose regolith in the younger southern hemisphere may also aid the formation of deeper craters (Vincent *et al.* 2013).

Topography plays a much more important role in crater formation and evolution on small bodies and moons than on terrestrial planets. For example, Vesta's ratio of observed relief to size (15%; Williams *et al.* 2013) is significantly greater than for terrestrial planets (1%; Jaumann *et al.* 2012). Strongly asymmetric craters have been seen on the many steep surfaces of Vesta (Fig. 6(c)). During impacts on steep slopes ejecta is prevented from being deposited in the uphill direction and slumping material superimposes the deposit of ejecta on the downhill side (Krohn *et al.* 2014). This leads to craters with a smoothed downslope rim that is often covered by the asymmetric ejecta (Jaumann *et al.* 2012). Resurfacing due to impacts, gravitational modifications and seismic shaking are important geophysical processes that not only add to the complexity of Vesta's surface evolution, but also substantially alter Vesta's morphology (Jaumann *et al.* 2012). Young bright and dark-rayed craters and their ejecta field are superposed across the surface of Vesta (Fig. 6(b); Williams *et al.* 2014; Yingst *et al.* 2014). Pond-like deposits are also seen on the surface of Vesta. Similarly to on Eros, they tend to have a downslope asymmetry within craters on slopes, and show no evidence for regolith flows into the craters and depressions (Jaumann *et al.* 2012; Cheng *et al.* 2002b). However, given the more important gravity on Vesta (compared to Eros) and the larger size of such pond-like features, their formation may simply be due to standard crater slumping, rather than

a process by which external material is transported into the crater.

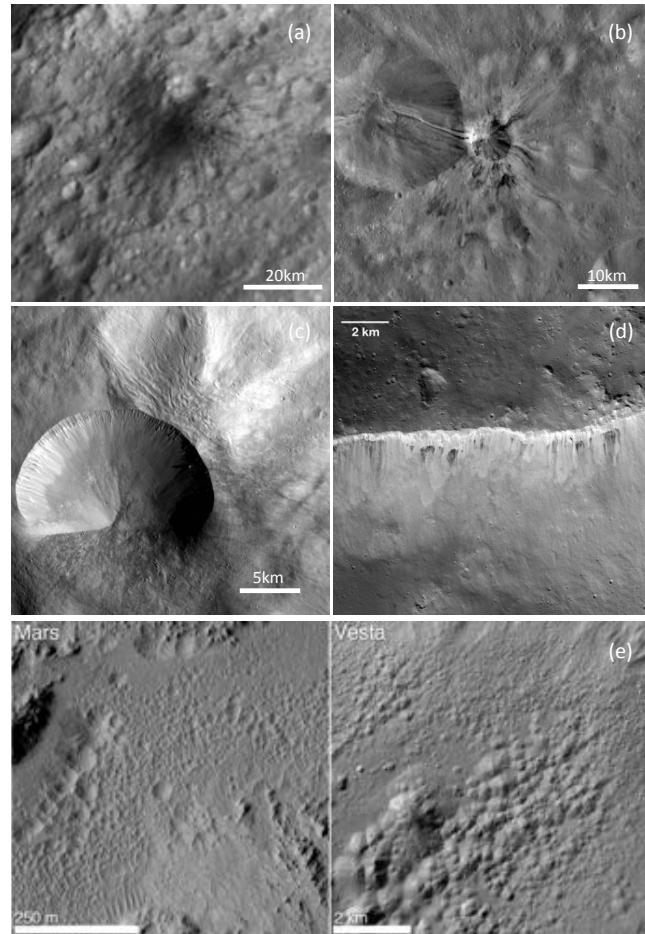


Figure 6: Surface processes on Vesta; (a) Dark hill (PIA14689, modified), (b) Fresh crater (center) with bright and dark rays (PIA15045, modified), (c) Crater on a slope with a sharp crest uphill and slumping material covering the lower rim PIA15495, (d) Dark and bright material at the rim of Marcia crater (NASA/JPL-Caltech/UCLA/MPS/DLR/IDA/LPI/ASU), (e) Pitted terrains on Mars (left) and Vesta (right) (PIA16185, modified).

**Evidence for an active regolith on Vesta -** As on the surfaces of the other asteroids discussed so far, extensive evidence of regolith mobility has been observed on Vesta; slumps of material, scarps beginning at the top of a slope, dark and bright material emanating from the rims or walls of impact craters, or running downslope into the crater bowl (Fig. 6(d); Jaumann *et al.* 2012; Williams *et al.* 2013; Yingst *et al.* 2014). Lobate, flow-like features are generally observed in close proximity to impact craters or in steep slopes (Williams *et al.* 2013). These features are interpreted as gravity-driven mass flow deposits, impact ejecta deposits or, for a small number of features, impact melt deposits (Jaumann *et al.* 2012; Williams *et al.* 2013).

On Vesta, the seismic shaking created by the giant basin forming impacts probably contributed to smoothing and erasure of small features well beyond the extent of the ejecta blankets (Vincent *et al.* 2013). Mixing of regolith materials (e.g., the dark exogenic materials with impact ejecta) is evident on Vesta’s surface (Jaumann *et al.* 2014; Pieters *et al.* 2012). There is also dearth of large-scale volcanic features on the surface of Vesta, compared to what was expected (e.g., Wilson & Keil 1996; McSween *et al.* 2011). Jaumann *et al.* (2012) suggest that the lack of such features may be due to extensive cratering, regolith formation and resurfacing that has removed the evidence of large-scale volcanism that ceased early in Vesta’s history (Williams *et al.* 2013; Jaumann *et al.* 2012). This will be discussed further in Section 5.

**Linear features on Vesta** - Large equatorial and northern troughs appear on Vesta’s surface (Fig. 1). The equatorial troughs are wide, flat-floored and bounded by steep scarps along  $\sim 240^\circ$  of longitude, while in the remaining longitude muted troughs, grooves and pit crater chains are evident (Jaumann *et al.* 2012). The northern troughs display gentler slopes, rounded edges and considerable infilling. This, combined with the heavy cratering, suggests that they are much older than the equatorial troughs (Jaumann *et al.* 2012). The centre positions of these circular troughs correspond to the centre of Vesta’s two southern basins indicating that the formation of the troughs and the basins are very likely related (see Fig. 2 of Jaumann *et al.* 2012).

### 3. AN INTRODUCTION TO GRANULAR MEDIA

Granular materials are unlike solids, in that they can conform to the shape of the vessel containing them, thereby exhibiting fluid-like characteristics. On the other hand, they cannot be considered a fluid, as they can be heaped (Gudhe *et al.* 1994). The study of granular dynamics is incredibly complex and constitutes an entire field of research by itself. In fact, P. G. De Gennes, a French physicist and Nobel Prize laureate, said that, “*For physicists, granular matter is a new type of condensed matter; as fundamental as liquid, or solid; and showing in fact two states: one liquid-like, one solid-like. But, there is yet no consensus on the description of these two states. Granular matter, in 1998, is at the level of solid state physics in 1930.*” (de Gennes 1999). This is not to say that granular matter has not been studied; ancient Egyptians did indeed know how to work with it, at least at an empirical level (Fall *et al.* 2014), Ernst Chladni (Chladni 1787) and Michael Faraday (Faraday 1831) studied the interaction of grains and fluids, and Geosciences have also long dealt with its complexities on the surface of the Earth.

On Earth we can observe granular materials involved in dramatic avalanches and rockslides, as well as active sand dunes moving across deserts. Industries also handle several different types of granular materials. Some examples are tablets or powders in the pharmaceutical trades as well as agricultural products such as wheat, oats, rice and other

cereals and sands in the construction industry. Theoretical models of granular dynamics are also widely employed to understand traffic flow and even crowd dynamics.

**What is a granular material?** The term granular material is most often used to describe a material containing a large number of particles that interact with each other through dissipative contact forces (Richard *et al.* 2005; Jaeger *et al.* 1996). In these aggregates, though each individual grain can be adequately described by Newtonian physics, a collection of grains offers complex behaviour which is often extremely sensitive to their external conditions (such as external forcing). A granular material is a material for which the relevant energy scale is the potential energy rather than the thermal energy i.e., particles in a granular material are massive enough for their potential energy to be orders of magnitude larger than their thermal energy (Schroter *et al.* 2005). For example, a typical grain of sand of mass  $m$ , raised by its own diameter  $d$ , in the Earth’s gravity  $g$ , will have potential energy  $mgd$  which is at least  $10^{12}$  times the thermal energy  $k_B T$  at room temperature on Earth (Jaeger *et al.* 1996).

The size of the constituent particles is closely linked to the type of interactions between the particles that will dominate the behaviour of the aggregate. On Earth the approximate size at which dissipative contact interactions dominate is  $100 \mu\text{m}$ ; at grain sizes  $< 100 \mu\text{m}$ , humidity and van der Waals forces will influence the particle interactions. Additionally, if present, the interstitial fluid will also influence the dynamics of the grains depending on the density of the fluid and the grain size (Burtally *et al.* 2002; Biswas *et al.* 2003). We will discuss in Section 4 how the importance of some of these forces changes in the low-gravity environment of an asteroid.

**Basic characteristics of granular materials** - Granular materials exhibit several characteristics that make them interesting but equally very difficult to model and understand. From the definitions presented above, some characteristics can be extracted, whilst others come from observation: (1) the grains that form a granular material are solid; (2) grain-grain interactions are highly dissipative; (3) potential energy, more than temperature, of the system is the relevant parameter; (4) granular materials are thixotropic; this means that they exhibit solid-, liquid- and gas-like behaviour; (5) friction, globally understood to be a combination of surface-surface friction and geometrical interlocking that prevents motion, makes aggregates able to sustain shear stress and contribute to the dissipative nature of grain-grain interactions.

From these basic characteristics, some phenomena result. For example, Fig. 7 (upper right) shows the solid, liquid, and gas flow regimes obtained in an avalanche-like situation. In a solid-like state, such as a heap or pile, the material is said to be “quasi-static” as the individual particles are in a stable mechanical equilibrium with their local

neighbours. In the liquid-like and gas-like states the material is said to “flow”. Dense flows (liquid-like state) are dominated by many-body interactions and occur when particles have long-lived contacts with many neighbours. In rapid or dilute flows (the gas-like state) there are no enduring contacts and the collision time is much smaller than the time between collisions (*Andreotti et al.* 2013 provide a thorough exposition of these topics).

Flowing granular materials can segregate according to particle properties (size, density, shape, and more) making granular media highly heterogeneous (Fig. 7 [upper left]). The phenomenon of segregation is a continued source of frustration for industries (*McCarthy* 2009), however, segregation may help us to explain several geological features observed on the surface of asteroids and discussed at the beginning of this chapter.

The final, but very important, property of granular materials is the non-linear transmission of force between particles via force chains. A force acting on a granular material is distributed through a complex force distribution network that depends on the positioning and packing of the individual particles. This grain network resists reorganisation when stressed and imposes a granular drag force when a solid object is pushed through the material (*Costantino et al.* 2008). Figure 7 (lower) shows the force chains inside a granular material. The presence of force chains can induce complex stresses at the sides of grain silos (*Schwartz et al.* 2012), preventing explosions at the bottom and instead leading to ruptures at the sides (*Janssen* 1895; *Jaeger et al.* 1996). This can be linked to the non-local effects granular materials exhibit (*Nichol et al.* 2010) and may even cause asteroids to feel long range consequences of small events such as meteoroid impacts (*Murdoch et al.* 2013b).

**Theoretical Frameworks** - As shown in the paragraphs above, granular matter can present solid-, liquid-, and gas-like behaviours, all at the same time. Although a complete theory to describe each behaviour simultaneously has yet to be put forward (e.g., (*Jop et al.* 2006; *GDR-MiDi* 2004)), different regimes (or states) can be modelled within certain frameworks. Depending on which of these theoretical frameworks is best-suited to the regime at hand, the properties of the grains will be described by different sets of parameters, e.g., friction, elastic moduli, viscosity, and restitution coefficients among others.

The elasticity-perfect plasticity models can be used for the static case (e.g., *Holsapple* 2004; *Holsapple & Michel* 2006). These models belong to the field of Continuum Mechanics and, as the name would suggest, they treat a granular media as continuous. This can be done under one assumption, the size of the grains that form the media (or soil) are very small compared with the typical length scale or the size of the sample. The dynamics of the media is modelled through yield criteria such as Mohr-Coulomb or Drucker-Prager in which the main parameters are angle of friction and cohesive strength. The pressure and shear stress (both

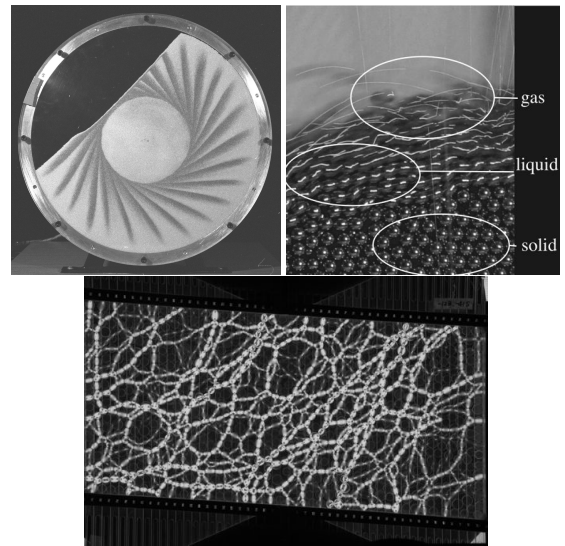


Figure 7: Top Left: Segregation of particles in a tumbler - The large sugar crystals (white) and small iron particles (black) segregate in the tumbler as described in *Gray & Chugunov* (2006). Credit: N. Gray, University of Manchester; Top Right: Solid, liquid or gas? - An illustration of the solid (bottom), liquid (middle), and gas (top) flow regimes obtained by pouring steel beads on a pile. Credit: O. Pouliquen and Y. Forterre; Bottom: Force chains in a granular material - Photoelastic image of a system that has been jammed by applying simple shear strain from an initially force-free state. The apparatus used here applies shear from the boundaries and also from the base, which consists of individual slats which deform affinely with the boundary. Credit: J. Ren and R. P. Behringer, Duke University.

derived from the principal stresses of the stress tensor) define the stress state of the media and are average quantities that in reality result from the contacts between particles and the interactions between their surfaces.

Fluid mechanics equations are used for dense flows, or for when grains begin to flow like a liquid (e.g., *Haff* 1983; *Forterre & Pouliquen* 2008). Within this framework, the dynamics of the medium is described through a continuity equation, derived from the conservation of mass principle; a momentum equation, derived from the conservation of momentum principle (in the case of granular materials, a description of viscosity must be included); an energy equation, derived from the conservation of energy principle; and an equation of state relating the three conservation equations.

Kinetic Theory (e.g., *Jenkins & Zhang* 2002; *Brilliantov & Pöschel* 2010), used for dilute, highly dynamical (gas-like) systems makes the following assumption: the particles only have binary collisions. Of course, in a real system this is not the case as multi-particle collisions may also occur; however, they are determined to be too rare to be taken into account. The validity of the assumption is re-

lated to the density of the granular system (must be safely below jamming density) and the duration of the collisions (must be short in order to avoid the occurrence of three or more particles in simultaneous contact). Thus, the particles of this system are idealised as hard spheres (instantaneous collisions). In this particular regime, the concept of granular temperature can be defined. A “granular temperature” can be defined in multiple ways, but essentially it is some measure of the average of energy fluctuations exhibited by a collection of grains. An example of one such definition, for a collection of  $N$  grains of average velocity  $\bar{\mathbf{v}}$  and average spin  $\bar{\boldsymbol{\omega}}$ , with each grain having a mass  $m_i$ , velocity  $\mathbf{v}_i$ , moment of inertia  $I_i$ , and spin  $\boldsymbol{\omega}_i$ , the granular temperature may be defined as

$$T_g = \frac{1}{2Nk_B} \sum_{i=1}^N \left( m_i |\mathbf{v}_i - \bar{\mathbf{v}}|^2 + I_i |\boldsymbol{\omega}_i - \bar{\boldsymbol{\omega}}|^2 \right). \quad (1)$$

This quantity does not include, but is analogous to, the thermodynamic temperature (Walton & Braun 1986). One important difference between a granular gas and a molecular gas is the inelastic nature of the collisions of the former, which leads to clumping and effectively serves to distinguish the behaviour of granular material.

#### 4. THE ASTEROID SURFACE ENVIRONMENT

By now it should be clear that asteroid surfaces are formed by regolith of various shapes, sizes, materials and, therefore, material properties. In a granular aggregate, these material properties are intrinsically related to the size and shape of the grains, their atomic and electronic structure, and the gravitational field to which they are subjected, to mention the most important factors. These properties will also play a role in how asteroids’ surfaces, and asteroids as a whole, react to external agents such as gravitational fields of other planetary bodies, solar radiation pressure (Yarkovsky and YORP effects, particle transport and levitation) or impacts. In what follows, we will explore these aspects of the surfaces of asteroids. Note that SI units should be assumed in all expressions in this section.

##### 4.1. Surface characterisation

**Materials** - Different mineral compounds form the regolith that is present in asteroid surfaces; they provide their spectral, thermal and some mechanical characteristics. The first two are obvious as they have to do with the absorption, transmission and reemission of energy (Mazziero 2009); the third comes from how regolith is formed as that would be a reflection of the hardness of the material, the crystalline structure and forces between the surfaces of grains in contact (adhesion, cohesion and friction).

At the moment what is known about the materials that make up asteroids comes from the meteorites that have crashed on Earth, from spectral observations and, more recently, from the samples brought from asteroid Itokawa by the Hayabusa mission. Through the research carried out on

the available samples, it has been found that asteroids are formed mainly by pyroxine, olivine, plagioclase and iron compounds. These materials have crystalline structures, and their detailed study belongs to the field of solid state physics or condensed matter physics.

**Observed regolith characteristics** - Section 2 in this chapter has already summarised the main observations and interpretations made about the slopes and grain size distributions on asteroid surfaces.

**Surface gravity** - Up to this point, in the description and characterisation of the surface regolith of asteroids, there are no big differences with what can be found on Earth. However, it is here where the similarities end as one of the most important factors affecting the dynamics of the regolith on asteroids is the ambient gravity; i.e., the sum of the local gravitational field and centrifugal forces due to the rotation of the asteroid. The calculated surface gravity of asteroids such as Itokawa and 1999 KW4 can be found in Yoshikawa et al. (this volume), Scheeres et al. (this volume), Scheeres et al. (2010) and Hartzell & Scheeres (2013).

These surface gravity calculations show some important features that are not common in our terrestrial experience: (1) gravity is  $10^3$ - $10^6$  times smaller than Earth’s gravitational field,  $g$ ; (2) the gravitational field is not always perpendicular to the terrain; and (3) relatively small displacements on the surface of a small body could mean big changes in the gravitational field. Among the main implications: escape speeds are in the order of cm/s; micro-meteorite impacts could transfer enough energy to generate surface or even global changes; stepping or landing on one of these aggregates could generate an ejecta field that could damage the instruments of a spacecraft or generate a local avalanche.

**Friction** - Intuitively, the idea of friction is that of a force that resists the relative motion of two bodies that are in contact. This resistance may appear in various ways; the work carried out by Bowden & Leben (1939), Bowden & Tabor (1939) and Bowden et al. (1943) and later summarised by Rao et al. (2008) suggested that asperities or projections on the surfaces of the bodies adhere to form junctions. Therefore, work must be done to deform and break these junctions, and this is accompanied by wear or erosion of material in the interfacial region. Additional work is associated with the deformation of the material in a larger region near the interface (plowing).

The first attempt to formulate a macroscopic friction coefficient is attributed to Coulomb (1776), who equated it to the tangent of the angle of repose, by defining it to be the ratio of shear and normal stresses on an inclined pile of sand. The seminal work of Bagnold (1954) and Bagnold (1966) found that the frictional force varied as the square of the shear rate for grain-inertial flow in the regime of rapid shear.

On the other hand, *GDR-MiDi* (2004) made it clear that the rheological properties of granular flows (friction, viscosity) depend on the shear rate i.e., on the dynamics, thus putting the work of Bagnold and collaborators into context.

*Mehta* (2007) recognises that the proper microscopic formulation of inter-grain friction remains an outstanding theoretical problem. In a granular material, it is not only the grain-grain surface friction that will determine the resistance of a grain to movement, or the resistance of the aggregate to be sheared and deform, but also the grains' shapes, geometrical interlocking, packing and size distribution; all these factors are usually pulled together in a single term: the angle of (internal) friction that appears in the Mohr-Coulomb (MC) or Drucker-Prager (DP) yield criteria.

Within the Mohr-Coulomb yield criterion, the angle of internal friction is defined as the arctangent of the ratio of shear to normal compressive stress at the stability limit (see Fig. 8). The MC criterion prescribes that shearing along any plane in a granular material cannot occur unless the shear stress ( $\sigma_s$ ) on that plane reaches a value proportional to the normal (compressive) stress on that plane:  $\sigma_s = \mu\sigma_n$ . The proportionality constant  $\mu$ , the friction coefficient, is written as the tangent of the friction angle  $\varphi$ :  $\mu = \tan(\varphi)$ . Thus, the friction angle is a material property. The DP criterion is based on similar physical ideas, but uses a linear dependence of an average shear stress, as measured by the  $J_2$  stress invariant, on the pressure (*Holsapple* 2013; *Chen & Han* 1988). Theoretically, if a material is cohesionless, the angle of repose corresponds to the angle of internal friction. On the other hand, for a cohesive aggregate, the angle of repose has to be such that is related to the cohesive strength of the material (see *Nedderman* (2005) for an in-depth explanation).

Cohesive forces (electrostatic and van der Waals are among the best known interactions) are kept in a different term and, within either criteria, do not affect the angle of friction, but only the angle of repose. Fig. 8 shows the relation between the normal stress ( $\sigma_n$ ), shear stress ( $\sigma_s$ ), cohesive strength ( $c$ ), tensile strength ( $\sigma_a$ ) and friction angle ( $\varphi$ ). If cohesive strength is defined as the shear stress at zero normal stress then tensile strength is the normal stress at zero shear stress.

On Earth, a well-know experimental fact is that angles of internal friction of cohesionless granular materials vary from 25° for smooth spherical particles to 45° for rough angular particles (*Carrigy* 1970; *Pohlman et al.* 2006; *Klein-hans et al.* 2011). Calculations made on asteroids Eros and Ida, and Martian satellites Phobos and Deimos show that only Ida has more than 2% (by area) of gravitational slopes above typical repose angles (35°). At this point it is worth explaining that the static angle of repose is the maximum slope that can be supported before the formation of an avalanche and a dynamic angle of repose is the slope that results after this avalanche has taken place. The maximum angle of stability, critical angle and static angle of repose are the same; angle of repose and dynamic angle of repose

are also the same. The static angle of repose may be related to cohesive forces including van der Waals forces, electrostatic forces and capillary forces in case of microscopic fluid pockets between the particles. Using a parabolic flight experiment *Klein-hans et al.* (2011) concluded that for decreasing gravity, the static angle of repose increases while the dynamic angle of repose decreased for all tested materials.

**Electrostatic forces and cohesion** - As mentioned before, any kind of cohesive force between the grains of an aggregate is going to increase the value of its angle of repose. This includes van der Waals, capillary, electrostatic and magnetic forces. The effects of these cohesive forces can be clearly seen in powders on Earth (flour, toner, pollen, chalk are common examples). How they appear and when they are apparent in the behaviour of granular aggregates will be discussed in the next sections.

## 4.2. Cohesive and adhesive forces

**Definition** - Cohesive and adhesive forces have the same origin, the only difference being that the term cohesive applies to the attractive force between molecules of the same material and the term adhesive applies to molecules of different materials. For example, liquid water molecules attract one another and form water droplets with surface tension (this is cohesion); water molecules and silica molecules also attract one another and water can make a glass wet (this is adhesion). These attractive forces are electromagnetic in nature and are appreciable when the electronic clouds of the atoms that form the surfaces of two bodies are within a few angstroms. The term van der Waals forces is used here very loosely and refers to the totality of nonspecific attractive or repulsive intermolecular forces other than those responsible for ionic and covalent molecular bonds (*McNaught & Wilkinson.* 1997). These interactions are often modelled by the Lennard-Jones potential

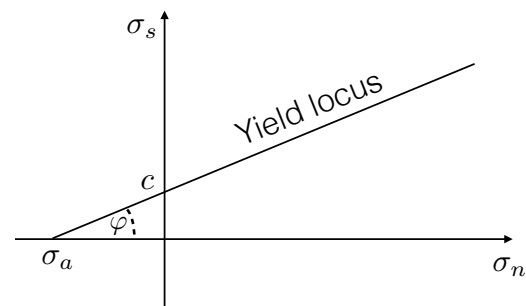


Figure 8: Mohr-Coulomb yield criterion: normal stress ( $\sigma_n$ ), shear stress ( $\sigma_s$ ), cohesive strength ( $c$ ), tensile strength ( $\sigma_a$ ) and friction angle ( $\varphi$ ).

(Jones 1924):

$$V_{LJ} = 4\epsilon \left[ \left( \frac{\gamma}{r} \right)^{12} - \left( \frac{\gamma}{r} \right)^6 \right] \quad (2)$$

where  $\epsilon$  is the depth of the potential well,  $\gamma$  is the finite distance at which the inter-particle potential is zero and  $r$  is the distance between the two particles (neutral atoms or molecules). Though other, more accurate forms of the potential exist, this one is usually used in computer simulations due to its simplicity. The  $r^{-12}$  term describes the Pauli exclusion principle due to overlapping electron orbitals and the  $r^{-6}$  term describes the long-range attraction (van der Waals force, or dispersion force).

Johnson *et al.* (1971), Heim *et al.* (1999) and Hughes *et al.* (2008) theoretically and experimentally studied the characteristics of the van der Waals force in granular materials. The cohesion between two spherical particles (radii  $r_1$  and  $r_2$ ) can be approximately described by (Castellanos 2005; Perko *et al.* 2001; Rognon *et al.* 2008):

$$F_c = \frac{A}{48(t+d)^2} \frac{r_1 r_2}{r_1 + r_2} \quad (3)$$

where  $A$  is the Hamaker constant for the grains ( $4.3 \times 10^{-20}$  Joules for lunar soil),  $t$  is the minimum distance between the particle surfaces due to adsorbed molecules and  $d$  is the width of any additional separation between the particles beyond that caused by the presence of the adsorbed molecules. In the extreme environment of space the minimum distance between the materials can be much closer than possible on Earth where atmospheric gases, water vapor, and relatively low temperatures allow for significant contamination of surfaces ( $d = 0$ ). These much cleaner surfaces and closer contacts allow for increased cohesion (Perko *et al.* 2001; Scheeres *et al.* 2010).

Perko *et al.* (2001) define a cleanliness factor  $S$  as  $\Omega/t$ , where  $\Omega$  is the diameter of an oxygen ion ( $O^{2-}$ ) and  $t$  is defined as above. This being so, the cohesive force between a grain (radius,  $r$ ) and a flat surface (or a much larger grain) is:

$$F_c = \frac{AS^2}{48\Omega^2} r \quad (4)$$

#### 4.3. Electrostatic forces

Electrostatic forces have been hypothesised to play an important role on the surfaces of asteroids, and have been specifically invoked as one means by which small dust grains can be transported across a body's surface. The first evidence of electrostatic lofting was the Lunar horizon glow observed by the surveyor spacecraft (Rennilson & Criswell 1974) at the terminator region. A second discovery contributing to this hypothesis was the existence of ponds on Eros and other asteroids even though it has been found that their apparent distribution could have an observational bias. Finally, there is also the fact that the Hayabusa mission was able to bring back samples of grains from asteroid Itokawa despite the malfunctioning of the sampling

mechanism (Yano *et al.* 2006). It has been proposed that the electrostatic interaction between charged particles and a possibly charged sampler horn helped collect the sample (Tsuchiyama *et al.* 2011). Whether or not dust levitation occurs on asteroids is still an open question, although it is undoubtable that surface grains on these bodies are subject to electrostatic forces. Unfortunately, as of yet, this is still not fully understood.

The electrostatic force felt by a particle on the surface of an asteroid is related to its location on the surface. The charge density at any point on the surface is the result of the difference between the number of electrons that are deposited on it by the solar wind and those that leave the surface due to photoemission. These two vary with the location of the surface and with time as the asteroid rotates and solar wind influences different areas of the surface. Photoemission and solar wind interaction depend on the solar incidence angle and a variety of plasma-related phenomena that vary with solar longitude, respectively. The resulting charge on the surface of the asteroid then influences the charging of the particle in question and influences the plasma environment (photoelectron and plasma sheaths) that will be experienced by the particle if it is lofted above the asteroid's surface (Scheeres *et al.* 2010).

If grains are idealised as spherical, and we make the same assumptions as Colwell *et al.* (2005) about the plasma sheet, it is then possible to demonstrate that for a particle of radius  $r$  (surface area,  $\Lambda = 4\pi r^2$ ), the electrostatic force that would provide lofting is:

$$F_{es} = \epsilon_0 E^2 \Lambda \approx 4\pi \epsilon_0 E^2 r^2 \Rightarrow F_{es} \approx 9 \times 10^{-9} r^2 \quad (5)$$

where  $\epsilon_0$  is the permittivity of vacuum and  $E$  is the electric field.

Recent theoretical analysis and experiments have shown that cohesion will play a role in dust levitation Hartzell & Scheeres (2011); Hartzell *et al.* (2013) and also that cohesion will dictate the electric field required for lofting for particles smaller than 1 mm on Itokawa (100  $\mu\text{m}$  on Eros and 10  $\mu\text{m}$  on the Moon). Furthermore, these experiments have also shown that a balance between cohesive, gravitational and electrostatic forces is needed to ensure levitation.

#### 4.4. The link between the surface environment and the geophysical features

In the previous sections we have tried to account for and describe the origin of the main forces that could affect grains on the surface of an airless planetary body. However, an even more interesting aspect is the interplay of these forces as this determines the dynamics of the grains and the landscape of the surface as a whole. With this in mind, and following the notation used by Scheeres *et al.* (2010), we define something called a *bond number* as:

$$B = \frac{F_c}{W} \quad (6)$$

where  $F_c$  is the cohesive force acting on a grain and  $W$  is its weight. For an ambient gravitational acceleration of  $g_A$  the

ambient weight of a grain is defined as  $W = mg_A$ , where  $m$  is the particle's mass.

On small planetary bodies, self-gravity between individual grains is much more important than on Earth and should be taken into account in calculations. For two equal-size particles of radius  $r$  and density  $\rho_g = 3500 \text{ kg/m}^3$  (larger than the asteroid's bulk density) the bond number is:

$$B_{self} = G \frac{4\pi\rho_g r}{3g_A} \approx 1 \times 10^{-6} \frac{r}{g_A}. \quad (7)$$

For the electrostatic force due to photoelectric emission alone, using eq. 5:

$$B_{es} = 6 \times 10^{-13} \frac{1}{g_A r}. \quad (8)$$

We note that triboelectric charging and other (not yet understood) mechanisms in the terminator regions could increase the electrostatic force to  $F_{es} \approx 0.1r^2$ . This would, therefore, increase the electrostatic bond number to:

$$B_{es} \approx 7 \times 10^{-6} \frac{1}{g_A r} \quad (9)$$

For cohesive forces and for material parameters of lunar regolith:

$$B_c = 2.5 \times 10^{-6} \frac{S^2}{g_A r^2} \quad (10)$$

where  $S$  is the cleanliness factor defined earlier.

On small planetary bodies, for sufficiently small grain sizes, these bond numbers can easily attain values greater than 1, meaning that the grain's own weight can be overcome. Strong cohesive forces give rise to highly porous structures first called "fairy castles" by *Hapke & van Hoen* (1963). Back then they attributed the existence of such structures to adhesive and long-range electrostatic forces that act between grains during deposition and influence their trajectories. After that, the work of *Matson & Nash* (1983), *Kreslavsky & Shkuratov* (2003) and *Cassidy & Johnson* (2005) shed more light on how these structures affect photometric anomalies of the Moon. Anomalous halos around small bright impact craters have been associated to changes in porosity probably related to some geologically recent damage of the equilibrium regolith structure.

Additionally, the scaling of cohesive forces with ambient gravity means that cm-sized grains in a microgravity environment may behave as  $\mu\text{m}$  size grains in Earth's gravity. Keeping this in mind, *Mériaux & Triantafillou* (2008) and *Durda et al.* (2013) have started research to understand the dynamics of cohesive powders under vacuum as a proxy to regolith-covered granular surfaces on asteroids. Simulations carried out by *Sánchez & Scheeres* (2014) and *Hirabayashi* (2014) have shown that modest values of cohesive strength (25 - 150 Pa) and a heterogeneous structure can drastically modify the maximum spin rates, disruption patterns and the existence or not of surface flow. The results obtained by *Rozitis et al.* (2014), *Hirabayashi et al.* (2014) and *Scheeres* (2014) about 1950 DA and P/2013 R3 seem

also to agree with the models, showing that values of cohesive strength under 100 Pa and angles of friction similar to those found on granular aggregates on Earth ( $35^\circ - 45^\circ$ ) are enough to explain the elevated spin rates of these asteroids.

## 5. GEOPHYSICAL PROCESSES ACTING ON ASTEROIDS

As we have already discussed, asteroids observed by spacecraft preserve records of geophysical processes that have operated at their surfaces and sometimes in their interiors. Here, these processes are classified into the following three categories: (1) exogenic phenomena, that are outer geophysical processes including impact cratering and slope failures/collapses, (2) endogenic phenomena, that are inner geophysical processes including ridges, faulting, and possible volatile and volcanic activities, and (3) other origins including tidal and YORP effects. Note that some processes dominantly acting on one asteroid might not necessarily act on other asteroids because the physical, especially mechanical, environments of asteroids vary significantly (for example, Vesta is considered to have been volcanically active because its mass is significantly large; 10 orders of magnitude larger than that of Itokawa, which is simply a pile of rubble).

### 5.1. Exogenic phenomena

Because of the lack of an atmosphere, an asteroid is directly exposed to solar wind, cosmic and solar rays and influxes of meteoroids of varying sizes. An impact can largely modify the shape of an asteroid and even its arrangement (such as impact-induced break-up of an asteroid). This will not be discussed here, rather, we focus on surface processes resulting from impacts.

On small bodies regolith is traditionally believed to result from repetitive impacts which excavate the surface and distribute ejecta materials. However, speeds of ejecta are typically greater than several tens of centimetres per second (*Housen et al.* 1979; *Housen & Holsapple* 2011), which corresponds to the gravitational escape speed of kilometre-sized asteroids. Impact debris reaccumulation, therefore, may not be solely responsible for the ubiquitous presence of regolith on small asteroids. Other regolith formation processes have been proposed including during contact-binary forming collisions of asteroids, by tidal forces, as well as the retention of regolith from a parent body (*Barnouin-Jha et al.* 2008; *Scheeres et al.* 2007). Using laboratory experiments and numerical simulations, *Delbo et al.* (2014) have shown that thermal fragmentation induced by diurnal temperature variations breaks up rocks larger than a few centimetres more quickly than comminution by micrometeoroid impacts. The latter was demonstrated by adapting the lunar impact induced comminution rates of *Hoerz et al.* (1975) to asteroids. Because thermal fragmentation is independent of asteroid size, this process can also contribute to regolith production on larger asteroids. Production of fresh regolith originating in thermal fatigue frag-

mentation may, therefore, be an important process for the rejuvenation of the surfaces of NEAs (Delbo *et al.* 2014).

Once formed, resultant deposits of loose debris will be affected by the gravity in a longer timescale, where repeated disturbances cause overall slow motion in the downhill direction. The disturbances may be caused by processes such as small impacts and severe thermal cycling, while many of the surface processes are in some aspects similar to those terrestrial phenomena resulting from expansion and contraction processes, heating and cooling, wetting and drying, and freezing and thawing. We note that here there are many important temperature-related processes occurring on asteroid surfaces and these are discussed in Delbo *et al.* (this volume).

**Impact ejecta mantling** - An impact will excavate the surface and create impact ejecta, which usually result in a deposit of debris surrounding the impact crater except for the cases in which the target has too little gravity to retain ejecta or too much porosity to produce it. The ejecta deposits normally affect at least the area within 5 crater radii by blanketing the original surface (Melosh 1989). In the case of gravity-dominated cratering, the thickness of the deposit,  $H_b$ , is given by

$$H_b = 0.14R_c^{0.74} \left[ \frac{r_c}{R_c} \right]^{-3}, \quad (11)$$

where  $r_c$  is the distance from the crater center and  $R_c$  is the crater radius (McGetchin *et al.* 1973). As suggested in this equation, the ejecta deposit is thickest at the crater rim and thins with increasing distance away from the crater. Impact-ejecta mantling may account for the absence of discernible surface features near craters on bodies such as Lutetia.

When the ejecta deposit is continuous and clearly recognised to be the result of the cratering event, it is called an ejecta blanket. However, such a blanket is not recognised on the surface of a small asteroid. Considering the low gravity, as well as the often irregular shapes, the above equation might not be directly applicable for small asteroids. In fact, other than the local gravity, spin parameters, especially the rotational period, can significantly affect the situation and cause very asymmetric ejecta blankets as observed on Eros. For example, a three-dimensional SPH (Smoothed-Particle Hydrodynamics) simulation of a hemispheric-scale impact onto Vesta, which spins every 5.3 hours, show that variably shaped, multiply folded deposits can be formed (Jutzi & Asphaug 2011) rather than a simple ejecta mantling.

The presence of boulders adjacent to an impact site on Lutetia suggests that boulder generation is a common feature of large impacts on this asteroid (Sierks *et al.* 2011). In fact, the fragments of ejecta deposits can be size-sorted through an impact event. Even though some interaction may occur between ejecta fragments in the denser parts of the ejecta curtain, general motion of the fragments is likely dominated by ballistics and thus follows a nearly parabolic trajectory above the asteroid before falling back to the surface. The size of the ejecta fragments near the base of the

ejecta curtain is expected to be larger than the fragments higher in the curtain.

One may wonder if ejecta may selectively escape from the surface of an asteroid never to return to mantle its original surface. This idea has been tested against the observations of Itokawa, for which 530 boulders larger than 5 m in size have been identified on its surface (Michikami *et al.* 2008). Assuming the slope value on the cumulative plot (Fig. 3) from Saito *et al.* (2006), the cumulative number ( $N$ ) of boulders may be approximated as:

$$N(> d) = 4.8 \times 10^4 d^{-2.8}, \quad (12)$$

where  $d$  is the diameter of a boulder. If we assume that the above size distribution is continuous down to the size of a pebble, the volume of pebbles (4 mm to 6.4 cm in size) can be estimated as  $1.9 \times 10^5 \text{ m}^3$ . Note, however, that smaller particles that exist on the asteroid surface are difficult to observe, because they are overlapped by larger boulders; the size distribution may, therefore, be different from that observed for larger boulders by 0.2-0.3 in the slope of log-log plot. This estimate is nonetheless of the same order as that estimated from the areas and depths of smooth terrains ( $2.3 \times 10^5 \text{ m}^3$ ; Miyamoto *et al.* 2007). It might, therefore, be appropriate to assume that no particular pebble-sized blocks have selectively escaped or accumulated (Miyamoto 2014).

**Seismic shaking** - Crater excavation resulting from an impact onto an asteroid is associated with a shock wave that severely shakes the terrain. Such shaking may induce local movements that cause a net downslope movement of loose surface material (Richardson *et al.* 2005) and this effect can be more important for a smaller asteroid because the seismic energy is unable to attenuate over a large volume.

Indeed, the first evidence for such seismic shaking on an asteroid was presented by Thomas & Robinson (2005). They showed that the formation of a relatively young crater (7.6 km in diameter) on asteroid Eros resulted in the removal of other craters as large as 0.5 km over nearly 40% of the asteroid's surface. As burial by ejecta cannot explain the observed pattern of crater removal, and the areas with low small-crater densities correlate well with radial distance from the Shoemaker crater, they conclude that seismic shaking is the most probable mechanism.

Assuming that the seismic energy is completely supplied by the kinetic energy of an impactor, the ratio of the maximum acceleration to the surface gravity,  $a/g$ , can be written as:

$$\frac{a}{g} = \frac{3fv_i}{G} \sqrt{\eta \frac{\rho_i D_i^3}{\rho_a^3 D_a^5}}, \quad (13)$$

where  $f$  is the seismic frequency in Hertz,  $v_i$  is the velocity of the impactor,  $G$  is the gravitational constant,  $\eta$  is the seismic efficiency factor (the fraction of the original kinetic energy converted to seismic energy),  $\rho_i$  is the bulk density of the impactor,  $\rho_a$  is the bulk density of the asteroid,  $D_i$

is the radius of the impactor, and  $D_a$  is the diameter of the asteroid. For the case of a rubble pile, the seismic energy may attenuate significantly. In this case, a diffusive scattering theory as adopted by *Richardson et al. (2005)* might be a realistic approach. In this theory,  $a/g$  on a diffusive body may be written as in Eq. (13) but multiplied by the scale factor  $\exp(-\frac{fD_a^2}{K\pi Q})$ , where  $K$  is the seismic diffusivity and  $Q$  is the seismic quality factor. Note that the exact values of some of the parameters for the above equations, such as  $f$ ,  $K$ ,  $Q$ , and  $\eta$  are difficult to properly obtain. However, most importantly, both models show that the size of an asteroid is an important factor to determine the surface acceleration against the gravity; smaller asteroids vibrate easier than larger asteroids. Although it is difficult to constrain reasonable ranges of values for many parameters, the above equations generally suggest that very small impactors may produce global shaking. Thus, repetitive impacts on asteroids may cause significant shakings, believed to be responsible for the depletion of craters on Itokawa and small craters on Eros.

**Mass movements** - Once an asteroid is seismically shaken, reverberation continues until internal friction and collisions finally convert it entirely into heat. Similarly, some other disturbances such as heating and cooling may occur. When the formation of faults, rapid landslides, or other processes occur releasing horizontal stress, such disturbances generally make the ground surface expand perpendicularly to the slope. When the disturbance ceases, the ground surface contracts along the direction of gravity, which is not necessarily parallel to that of the above surface expansion (especially on a surface inclined against the local gravity). When such expansion and contraction occur cyclically, the materials covering the surface show overall migrations, which are essentially downslope displacements. This kind of downslope mass movements of dry, unconsolidated material is a common geological process on terrestrial planets (*Meunier et al. 2013*). However, geophysically, those on terrestrial planets are generally interpreted in terms of the competition between gravity or inertia and inter-granular friction. Naturally for the case of a relatively smaller asteroid, the situation may be more complicated since other forces such as cohesive forces can play a significant role, as discussed in Section 4.

A slow and cyclic creep process is not the only type of mass movement on an asteroid. More rapid examples include landslides, which take place when the acceleration due to the ambient gravity exceeds the ability of a rock on a slope to resist. Roughly speaking, the conditions for this phenomenon to occur can be described by Coulomb's equation,  $\sigma_s = c + \sigma_n \tan \varphi$  (see Fig. 8). If the shear of a block of rock exceeds the maximum sustainable shear stress, the block slips and may be recognised as a landslide. This kind of mass movement can be found as small-scale, streak-like features such as observed on crater walls of Vesta (Section 2). Indeed, mass movements can expose an interior, often

recognised through differences in colour, as described in Section 2.

When a block of rock slips on a slope, sometimes the balance of shear stress and sustainable shear stresses inside the block changes. This causes a flow-like phenomenon, sometimes referred to as a debris flow or granular flow (*Legros 2002*). Some of the above-mentioned mass movements may be better explained by this process.

When we consider a case in which a block of rock is resting on a slope at angle  $\alpha$ ,  $\sigma_s = (\frac{mg}{A}) \sin \alpha$ , where  $m$  is the mass of the block and  $A$  is its basal area. Similarly,  $\sigma_n = (\frac{mg}{A}) \cos \alpha$ . Assuming the case in which the sliding rock is actually loose debris (a case in which cohesion is negligible in a terrestrial environment, and thus flow occurs rather than simply sliding), the largest shear stress in the block is achieved at the base of the rock. In this situation,  $\sigma_s = \sigma_n \tan \varphi$ , which gives the condition of  $\alpha = \varphi$ . In other words, in this case, the angle of repose is the same as the angle of internal friction and is independent of the gravitational acceleration.

The overall migrations of such flows are sometimes considered as gravity flows, whose speed  $U$  may be described as  $U \sim D(\rho gh)^{1/2}$ , where  $D$  is a coefficient of drag force,  $\rho$  is the density of the flow, and  $h$  is the thickness of the flow. The speed of the flow, therefore, depends on the square root of gravity (*Jop et al. 2006*), indicating that the flow can be much slower than typical ones on Earth.

Another type of mass movement is electrostatic dust levitation (see also Section 4), which is proposed to be responsible for particle migrations on airless bodies exposed to both direct sunlight and the solar wind (*Lee 1996*). Smaller levitated particles on an asteroid may escape into space through the solar wind, but larger particles may settle back onto the surface. This may explain the smooth ponds on the surface of Eros (*Robinson et al. 2001*), the formation of which clearly involves the settling of fines ( $\ll$  cm-sized particles) in gravitational lows by a secondary process, after crater formation (Section 2 *Cheng et al. 2002b*; *Robinson et al. 2002*).

*Cheng et al. (2002b)* suggest, however, that the pond material derives from the flanks of the bounding depression seismically shaken down to the bottom of the depression. Another idea for the formation of ponds is eroding of boulders; repeated day/night cycling causes material fatigue leading to erosion of the boulders (*Dombard et al. 2010*). However, recent morphological analyses indicate that the deposited material most likely originates from a source external to the ponds themselves (*Roberts et al. 2014a*). In addition, the morphology, geography, colour and albedo of the ponds may be consistent with formation by electrostatic levitation rather than seismic shaking (*Riner et al. 2008*; *Richardson et al. 2005*).

**Regolith segregation** - In addition to the size segregation that occurs during impact ejecta mantling, in granular flows where particles have different physical properties, particle

segregation also occurs (as discussed in Section 3). One example of such segregation is in a granular avalanche. The dominant mechanism for segregation in granular avalanches is kinetic sieving (*Bridgwater 1976*) rather than effects of diffusive remixing, particle-density differences, or grain-inertia (*Thomas et al. 2000*). As the grains avalanche downslope, there are fluctuations in the void space and the smaller particles are more likely to fall, under gravity, into gaps that open up beneath them because they are more likely to fit into the available space than the coarse grains. The fine particles, therefore, percolate towards the bottom of the flow, and force imbalances squeeze the large particles towards the surface (*Gray & Chugunov 2006*).

A further example of regolith segregation, that may be responsible for the presence of large boulders on the surface of asteroids such as Itokawa and Eros (*Asphaug et al. 2001; Miyamoto et al. 2007*), is the “Brazil-nut effect” (*Rosato et al. 1987*). The idea is that seismic shaking may cause the larger regolith particles to move up to the surface. If this is the case, the interiors of rubble-pile asteroids having experienced this kind of evolution are likely to be composed of smaller particles than those observed at the surface. This may also lead to some variations of macro-porosity with depth inside the asteroid.

The mechanism driving the Brazil-nut segregation is still under debate (*Kudrolli 2004*). It has been suggested that the segregation may result from the percolation of small particles in a similar fashion to the kinetic sieving mechanism, but here the local rearrangements are caused only by the vibrations (e.g., *Rosato et al. 1987; Williams 1976*). However, other experimental results from *Knight et al. (1993)* have shown that vibration-induced size segregation may arise from convective processes within the granular material and not always from local rearrangements.

Granular convection is, in fact, a process often invoked by the community of small-body scientists to interpret the surface geology of asteroids (*Miyamoto et al. 2007; Asphaug 2007*). However, as discussed in *Murdoch et al. (2013b)*, kinetic sieving and granular convection are strongly dependent on the gravitational acceleration (*Thornton 2005; Murdoch et al. 2013c*). A weak gravitational acceleration may, therefore, reduce the efficiency of particle size segregation. Indeed, recent numerical simulations and parabolic flight experiments of the Brazil-nut effect have shown that the speed at which a large intruder in a granular material rises is reduced as the external gravity decreases (*Tancredi et al. 2012; Güttler et al. 2013; Matsumura et al. 2014*). Therefore, all convective and particle segregation processes in a granular material on or near the surface of a small body may require much longer timescales than the same processes would require in the presence of a strong gravitational field

## 5.2. Endogenic phenomena

For terrestrial planets, “endogenic processes” are geological processes associated with energy originating from

the interior of the planet, including tectonics, magmatism, metamorphism, and seismic activities. However, in the case of asteroids, the ultimate cause of tectonics or seismic activities may be difficult to clearly separate.

Internal magmatism and volcanic processes are not often expected to occur on asteroids. However, differentiated early-forming asteroids should have experienced various kinds of volcanic activity, especially as a result of incorporating the heat-generating isotope  $^{26}\text{Al}$ . The howardite-eucrite-diogenite (HED) class of meteorites, whose parent body is believed to be the asteroid Vesta, have been studied in detail, and the magmatic origins of these rocks and their compositions as surface lavas or intrusions are well understood (e.g., *Taylor 1993*). Nevertheless, observations of Vesta show no conclusive evidence of volcanic features. The surface of Vesta, particularly the northern hemisphere, appears to be saturated with craters  $>10$  km in diameter (*Marchi et al. 2012*). This indicates that the surface regolith to depths of more than 1 km is significantly overturned. On the other hand, *Wilson (2013)* predicted typical lava flow dimensions are  $\sim 10$  m thick, much shallower than the thickness of overturned regolith, which might be the reason for the lack of clear evidence of lava flows or pyroclastics on the surface of Vesta.

Even though volcanism is not a common process on an asteroid, some features indicate phase-changing of materials and their transportation to the surface. Possible melting flows identified on Vesta might be good examples. Also, more than 10 active (mass-shedding) asteroids have been reported (*Jewitt 2012*) and the possible mechanisms for producing mass loss include dehydration stresses and thermal fracture. Although comets are not the focus of this chapter, we note that, in fact, strange features exist in the nuclei of both Tempel 1 and Wild 2. These features are interpreted as pits and scarp retreats resulting from venting of subsurface volatiles (*Veverka et al. 2013*).

Some pitted terrains of Vesta (Fig. 6(e)) are also believed to be related to subsurface volatiles; morphologic similarities of pitted terrains between Mars and Vesta suggest volatile release as an origin. However, because meteorites thought to originate from Vesta indicate low endogenic volatile content, it has been suggested that the volatiles have been delivered to Vesta’s surface and are not endogenic. The source may be carbonaceous chondrites, which have been observed as clasts in howardites (meteorites most likely originating from the surface of Vesta), or perhaps comets. Later impacts into this water-bearing regolith would result in devolatilisation due to impact heating and melting (*Denevi et al. 2012*).

Tectonic features are surface features created by internal stresses that fracture or deform the surface layer. Numerous tectonic features are documented on asteroids. For example, Vesta displays examples similar to those found on small Saturnian satellites such as Iapetus. Also, Rahe Dorsum on Eros is a ridge that extends for about 18 km around the asteroid, which resembles thrust fault structures on the terrestrial planets (*Prockter et al. 2002*). Tectonic deforma-

tion cannot occur without forces to drive it. However, many sources of tectonic stress exist of both internal and external origin, and a clear separation and exclusive classification is difficult.

For example, on Eros, the large “spiral” pattern southwest of Psyche, is suggestive of extensional tectonics whereas the spatial distributions of other ridge systems, as well as its estimated shear strength, indicate that the ridges are in fact thrust faults, which were formed by impact-induced compression (Watters *et al.* 2011; Cheng *et al.* 2002b; Veverka *et al.* 2000). However, the ridge system on asteroid (2867) Steins (hereafter simply Steins), which is the most prominent feature recognised on its surface, may be formed through the change in rotation rate due to the effect of solar radiation known as the YORP effect. The effect spins Steins, making the surface seek for the object’s potential-energy minimum, which may cause tectonic arrangements or landslide-like surface modifications towards the equator (Harris *et al.* 2009). Either process can explain the formation of the ridge at the equator. A similar origin is proposed for an equatorial ridge of 1999 KW4 (Walsh *et al.* 2008).

Grabens or linear depressions are found on many asteroids (see Section 2), which may seem strange given the fact that asteroids are covered by loose fragmental debris. It is possible that these fractures are evidence of competent rock below the regolith. It has been suggested that they result from stresses from large impact events, which have refocussed and caused fracture far from the crater (Fujiwara & Asada 1983; Asphaug *et al.* 1996), or that they are due to thermal stresses (Dombard & Freed 2002) and/or body stresses induced by changes in spin. However, faulting can occur even in a granular matrix when it is cohesive relative to the applied stress.

Grooves have been reported on Gaspra, Eros, Steins, Lutetia, and many other asteroids observed at high resolution. A subset of the grooves appear to be chains of pits (or crater-like indentations) in an almost linear arrangement. The global extent of a series of pitted chains found on Steins indicates these are not impact craters, because the chances of formation of many chains of these craters of similar size is highly improbable. Instead, partial drainage of loose surface material into a fracture within stronger, deeper material is considered as a likely origin (Richardson *et al.* 2002; Keller *et al.* 2010). This explanation of how pitted grooves form was suggested to explain the features seen on Phobos (Thomas *et al.* 1979). Experiments have demonstrated that, in such a model, the spacing of the pits along the groove is equal to the thickness of the regolith in which they form and is independent of regolith bulk density, grain size, shape, angularity and angle of repose (Melosh 1989; Prockter *et al.* 2002). Short and well-defined grooves can also be caused by a boulder that has bounced and rolled a short distance, but very few (<5) such tracks have been positively identified on the surface of Eros (Prockter *et al.* 2002; Robinson *et al.* 2001).

### 5.3. Tidal and rotational effects

There might be some morphological or even larger modifications of asteroids due to tidal forces. Modest influences are expected to include exposing layers of surface materials; to explain the fact that the laboratory spectra of ordinary chondrite meteorites are a good match to Q-type asteroids, Binzel *et al.* (2010) and Nesvorný *et al.* (2010) pointed out the possibility that Q-type NEAs underwent recent encounters with the terrestrial planets and the tidal force exposed fresh ordinary chondrite material on the surface. More considerable outcomes may include splitting the asteroid into a binary (Walsh & Richardson 2008) or even catastrophically disrupting it in a manner similar to comet Shoemaker-Levy-9 at Jupiter. Such tidal effects by a terrestrial planet are considered as one of the most likely creation scenarios for asteroid families (Fu *et al.* 2005). Also, strange shapes of some NEAs as revealed by radar images may have resulted from the tidal disruption processes and re-accumulations of disrupted fragments (e.g., Bottke *et al.* 1999).

YORP can modify both the rotation rate and the spin-axis orientation of small asteroids and has been identified as an important process driving their physical and dynamical evolution (Vokrouhlický *et al.* 2003). Asteroids of 5 km and smaller in radius in near-Earth orbits and a few tens of km in the inner main belt are subject to the YORP effect. The spin-up of asteroids can have dramatic consequences (Scheeres *et al.* 2007; Walsh *et al.* 2008). For example, the deficiency in small craters on Steins is attributed to surface reshaping (through landslides) due to spin-up by the YORP effect (Keller *et al.* 2010). The shape of the northern hemisphere of Steins is reminiscent of that of the NEA 1999 KW4, which has been attributed to spin-up by the YORP effect. A plausible scenario is that Steins was spun-up by YORP, leading to material sliding toward the equator to form the typical top-shape (Keller *et al.* 2010). Mass shed from the equator of a critically spinning asteroid can accrete into a satellite (Walsh *et al.* 2008). Alternatively, an asteroid may spin-up by the YORP effect until it reaches its fission spin limit and the components enter orbit about each other (Scheeres *et al.* 2007). Asteroid pairs may be formed by the rotational fission of a parent asteroid into a proto-binary system, which subsequently disrupts under its own internal system dynamics (Pravec *et al.* 2010). These binary asteroid formation mechanisms may explain the fact that asteroid pairs ubiquitously exist. For more information on asteroid binaries see Walsh *et al.* (this volume).

## 6. INVESTIGATING REGOLITH DYNAMICS

Regolith processes on asteroid surfaces may not have ready terrestrial analogs. In order to study regolith dynamics in the unique asteroid environment described in Section 4, both experimental methods and numerical simulations can be used.

## 6.1. Experimental methods

**Creating reduced-gravity conditions** - One of the major challenges for investigating the behaviour of regolith at the surface of an asteroid is to recreate the proper gravitational conditions. Microgravity, the condition of relative near weightlessness, can only be achieved on Earth by putting an object in a state of free-fall. Here we introduce some of the techniques used to perform experiments in reduced-gravity conditions.

Drop towers have been extensively used for microgravity experiments related to dust and regolith dynamics (e.g., *Hofmeister et al.* 2009 studying granular flow under reduced-gravity, and *Schräpler et al.* 2012 and *Beitz et al.* 2011 investigating low-velocity collisions between dust agglomerates). Parabolic flights can also provide a microgravity environment for regolith experiments (e.g., *Murdoch et al.* 2013a,c performing experiments of granular shear and granular convection, *Güttler et al.* 2013 investigating granular convection and the Brazil-nut effect, and *Dove & Colwell* 2013 investigating particle charging and the dynamics of charged particles on the surfaces of airless bodies). Such flights are normally operated using modified commercial aeroplanes, however, smaller aircraft have also been used (e.g., *Kleinhans et al.* 2011). Other ways of achieving microgravity are using a sounding rocket (e.g., *Krause & Blum* 2004 studying the formation of dust agglomerates) or flying an experiment on the International Space Station (e.g., *Colwell* 2003 investigating low-speed impacts into dust). Further methods of simulating microgravity exist such as magnetic levitation and neutral buoyancy. However, to perform an experiment with particles using these techniques, every particle in the experiment would have to be neutrally buoyant or magnetically levitated. If, for example, only the experiment container is levitated or buoyant, the individual grains would still feel the gravitational field.

**Creating the electrostatic environment** - The electrostatic part of the asteroid environment is provided by the solar wind, which is essentially a stream of plasma (electrons and protons) that originates in the upper atmosphere of the Sun. The energy of this plasma ranges between 1.5 and 10 keV. Though there are many ways to obtain plasma, the one technique that is chiefly employed to study lunar and asteroid environments uses an emissive filament within a cylindrical stainless steel vacuum chamber. Argon plasma is created by the impact ionisation using electrons emitted from a negatively biased and heated filament in the bottom of the chamber (*Wang et al.* 2012; *Hartzell et al.* 2013). However, the experiments have a higher density and lower temperature than the solar wind.

Efforts are being made to improve these experimental techniques so that the obtained results are not only qualitatively, but also quantitatively correct, and so that they can be directly translated to the asteroid environment. In spite of this, they carry size, time and cost constraints, and even

in the best possible conditions, at times they fall short of the real environments that are the object of study. These constraints are what make computer simulations, their development and understanding, attractive from a scientific point of view. Computer simulations of course also have a cost as there are many simplifications and assumptions that have to be made (see Section 6.2). This means that there must be a trade off between their complexity and their realism. A trade off that calls for a very careful look at the results and their interpretations as computational artefacts must be distinguished from fact. If research is carefully conducted, simulations can be used to guide better experiments and predictions of simulations can be tested so that nature is understood.

## 6.2. Numerical methods

With advances in computer hardware and software, numerical modelling has become increasingly important to the study of granular systems in general, and to granular systems in exotic environments such as the surfaces of small bodies, where conditions are difficult to replicate experimentally. The different types of numerical approaches can be divided into the broad categories of continuum and discrete. In the realm of numerical simulation, continuum approaches and discrete approaches have their relative advantages and disadvantages that depend on the specific investigation at hand. In general, discrete approaches attempt to treat material as individual particles, sometimes with large particles as proxies for groupings of smaller ones. Continuum approaches average the physics of nearby particles, and use smooth transitions to account for variance. Continuum approaches are particularly well suited for high-speed collisions, where material phase changes and the finite propagation speed of sound waves are important. In low-speed granular regimes, however, discrete approaches have the advantage of being able to capture the inherently discrete nature of granular systems and of being able to describe in great detail the properties of individual grains. These properties are then used to solve for the frictional and cohesive forces that arise when grains come into contact with each other. Discrete codes are also much better suited towards capturing the physics of slowly evolving granular systems such as those that take place on the surfaces of small bodies.

### 6.2.1. Numerical modelling of granular systems in planetary science

For many years, numerical continuum approaches have been used to address issues related to granular dynamics in the field of planetary science (e.g., *Holsapple* 1993, investigating scaling laws for impact-induced catastrophic disruption, and *Benz et al.* 1994, investigating different classes of two-body collisions). Continuum approaches have since grown significantly in sophistication (some in current use for the modelling of asteroid shapes and the scaling laws for disruption are, e.g., *Holsapple & Michel* 2008; *Holsap-*

ple 2009 and Sharma *et al.* 2009). Discrete numerical approaches, described below, have been in use in the field of planetary science since, e.g., *Brahic (1975); Brahic (1977)*, who simulated Saturn’s rings, *Asphaug & Benz (1994)*, who simulated the breakup of comet Shoemaker-Levy-9 using a soft-sphere discrete element method (SSDEM), and *Richardson et al. (1998)*, who conducted a more generalised numerical investigation into tidal breakups of small bodies using a hard-sphere discrete element method (HSDEM). In light of advances in computer processor speeds, only quite recently have robust versions of SSDEM begun to be applied to the realm of planetary science, and specifically to the study of regolith dynamics in microgravity environments. SSDEM granular physics codes are now developed or adapted specifically for planetary applications by various groups (e.g., *Wada et al. 2006; Sánchez & Scheeres 2011; Schwartz et al. 2012; Tancredi et al. 2012*) using various integration schemes and strategies to account for the types of friction between grains. Other codes, using continuum approaches, have also been developed to investigate, for instance, collisions between porous aggregates (*Sirono 2004; Jutzi et al. 2013*). However, owing to the granular nature of the relevant dynamical processes involved, the regolith surfaces of small bodies are more commonly modelled using discrete element methodologies, specifically (although not exclusively) SSDEM.

### 6.2.2. *The continuum approach to regolith modelling*

Continuum numerical modelling of granular material usually begins by defining a systematic approach to averaging the physics across many particles (and thereby treating the granular material as a *continuum*). The approach typically will involve dividing a parameter space or dimensional space into regions, and then integrating the system forward in time.

In describing fluid mechanics equations for dense flows, relevant conservation laws are followed, often in a Navier-Stokes framework (e.g., *Haff 1983*). At minimum, these conservation laws should include mass conservation, momentum conservation, and the conservation of energy together with the first law of thermodynamics. These regions may be described in Eulerian terms, where a volume in space is held constant, with material passing in and out of this volume, or in Lagrangian terms, where a region is described by the material itself as it moves around in space (e.g., see *Springel & Hernquist 2002* for a fully conservative derivation of a Lagrangian treatment in a SPH code). The numerical viscosity problems that stem from continuum codes (a known problem since *von Neumann & Richtmyer (1950)*, a result of the homogenising of material properties) are somewhat easier to mitigate in Eulerian approaches (*Springel 2010*), whereas the principle advantage to the Lagrangian approach is that the resolution of the system adjusts automatically to the movement of the material (see, e.g., the *Benz et al. 1994* handling of two-body collisions). Sophisticated codes that use hybrids of Eulerian and

Lagrangian descriptions, together with complex physical laws and computational parameters, have been developed (see *Monaghan 1988* for an early perspective). In addition, there have been significant advances in continuum coding approaches that mitigate some of the problems of numerical viscosity, including sophisticated differencing schemes (see, e.g., *Martí & Mulet 2014*).

In the modelling of granular media, the continuum approach often treats the material as a deformable solid and models it with some chosen finite-element (e.g., *Crosta et al. 2009*, who make use of the definition of bulk plastic and elastic moduli) or mesh-free (Lagrangian) method suited for the particular situation at hand (e.g., *Elaskar et al. 2000*). Stability problems (e.g., the stability of granular piles or cliffs) require an elasto-plastic framework that defines, at minimum, some type of yield criterion (consider the simple 1-D coulomb yield criterion: conditions are static until the tangential force exceeds the product of the coefficient of static friction and the normal force).

Depending on the system, a continuum approach could incorporate viscosity in some useful form (e.g., *Lagrée et al. 2011*) and treat the material as a fluid and use computational fluid dynamics (useful in describing outflows from, e.g., crater walls). However, since successful simulations of asteroid surface dynamics entail the capturing of the discrete nature of individual particles, the effects of such homogenisation must be examined thoroughly. *Haff (1983)*, in his article describing his efforts to treat granular media as a fluid analytically, considers many of the potential hazards and payoffs of using fluid dynamics from his analytical approach. These same considerations that arise analytically (i.e., the sharp boundary conditions on grain surfaces, including the complex frictional forces at play on these surfaces), also arise numerically.

### 6.2.3. *The discrete approach to regolith modelling*

The discrete-element method (DEM) is a general term applied to the class of discrete approaches to the numerical simulation of particle motion, where particles usually represent actual grains (or collections of grains), unlike the continuum approach that uses averages to homogenise the material. However, as continuum approaches use homogenisation schemes to simplify the complex and rapidly varying physical quantities within a material, in discrete approaches, the physics within individual particles are averaged, and thus the particles are defined only by their *effective* behaviour, described by quantitative parameters. Nevertheless, these parameters are typically borrowed directly from continuum mechanics, either by explicitly defining quantities such as the Poisson’s ratio and the Young’s, bulk, and shear moduli, or by using derived quantities including spring constants and friction coefficients.

DEM collisional routines are typically built off of an *N*-Body routine. In an *N*-Body framework, at the beginning of each timestep, forces on each of the *N* number of particles (bodies) in a given simulation are solved for and used to

advance the simulation ahead through time in small quantized *steps*. These forces can include, for example, external gravity or electromagnetic fields, and can incorporate the effects that the particles themselves have on the field (e.g., interparticle gravity). The collisional routines are then built on top of this framework, and define a new set of forces to account for the physical interactions that particles have with each other (of course these interactions are also electric at the molecular level).

In the standard implementation, particles are approximated as having perfect spherical geometry (more complex geometries are also possible). Since DEMs tend to compute the motions of large numbers of individual particles, it is relatively computationally intensive, which tends to limit either the length of a simulation or the number of particles in the simulation.

#### **The hard-sphere discrete-element method (HSDEM) -**

The numerical approach to solving the equations of motion in HSDEM is to discretise the simulation in time, with variables progressing in small steps (timesteps) by forward advancing along derivatives. Collisions are predicted in advance by analysing particle motion and checking for potential contacts that may occur within the current timestep. Particles are not allowed to penetrate each other (overlaps are not allowed). HSDEM codes carry out collisions between spheres by treating collisions as instantaneously occurring at a single point of contact that lies on the particles' surfaces; the sound speed through a particle is also instantaneous. Thus this methodology treats motions and mutual interactions of non-deformable, indestructible (hard) particles. The assumption of hard particles allows collisions to be carried out analytically, with post-collision velocities and rotations given by, e.g., *Richardson (1994, 1995)*.

#### **The soft-sphere discrete element method (SSDEM) -**

SSDEM is commonly used in the study of granular materials, and has often been applied to industrial problems (e.g., *Tsuji et al. 1992; Cleary & Sawley 2002; Kosinski & Hoffmann 2009*). The methodology has been applied in other disciplines of physics, such as chemical physics, under the name of Molecular Dynamics (MD), where it is used to compute motions of atoms and molecules and interactions between them (in fact, this application and nomenclature predates SSDEM's use in granular physical contexts; *Alder & Wainwright 1959*). In the complex case of simulating regolith dynamics, one must treat each of the relevant frictional forces by generalising and applying the rules of interaction between grains. The basic methodology having been developed by *Cundall & Strack (1979)*, SSDEM treats macroscopic particles as deformable spheres, allowing overlaps between particles to act as proxies for actual deformation. Particles are taken to be in contact if and only if their surfaces are touching or mutually penetrating. The greater the extent of this penetration, the more repulsive force is generated. The majority of codes either assume a

linear force dependence or a Hertzian dependence on penetration depth ( $F \propto x$  or  $F \propto x^{3/2}$ , where  $x$  is the penetration in units of length). Once a contact is established, particles are subject to frictional forces often making use of material parameters based on continuum mechanical theory; these forces will vary depending on the specific SSDEM code (see *Radjai & Dubois 2011* for a comprehensive overview on the different classes of SSDEM codes and common variations).

#### **6.2.4. Benefits and drawbacks between these numerical approaches**

In contrast to HSDEM, where collisions are solved for analytically, based on the positions and momentum states of the particles along with some basic material parameters to describe the behaviour, SSDEM must resolve each collision numerically. As such, collisions typically require dozens of timesteps to resolve. In HSDEM, however, since collisions are predicted in advance and then treated as instantaneous, it is the external dynamics (e.g., gravity) that drives the choice in step size rather than the collision handling; although the timestep may also be limited by concerns over missing a collision, timesteps in SSDEM can often be smaller than those used in identical HSDEM simulations by factors of  $10^2$ . In dense regimes, however, the speed of the integration in HSDEM is typically limited by collisional bottlenecks owing to the fact that collisions must typically be computed one-at-a-time in sequence, limiting the efficiency of parallel processing.

During the finite amount of time that it takes for two real particles to collide, the particles are in contact, exchanging energy and momentum. In sufficiently dense regimes, a third particle may intrude on this collision by making contact with either particle or with both particles, changing the outcome. This exposes another drawback of HSDEM's treatment of collisions between particles: multiple contact effects are not taken into account in HSDEM, where collisions are separate and instantaneous. Multi-contact systems of rigid, indestructible particles can, however, be solved using an algorithm known as contact dynamics (CD), which treats these rigid particles as subject to Coulomb static frictional forces (*Moreau 1994*). HSDEM also must account for the problem of *inelastic collapse*, which occurs when a group of particles collides infinitely often in a finite time, causing the simulation to grind to a halt (see, e.g., *Petit & Henon 1987; Bernu & Mazighi 1990* for early numerical encounters of this effect, and, e.g., *McNamara & Young 1992; McNamara 2000* for more complete quantitative descriptions). Although sophisticated collision-handling schemes have been tailored to help mitigate this problem (*Petit & Henon 1987; Luding & McNamara 1998*), the simplest way to avoid the finite-time singularity in HSDEM is straightforward: it requires setting some minimum impact speed or energy under which the coefficient of restitution is unity (no dissipation). This results in particles, even those in "stable" configurations, to always maintain some minimum energy

state (temperature), which may not appropriately capture certain low-energy granular regimes. Problems of inelastic collapse do not arise in SSDEM or CD methodologies.

SSDEM is nevertheless the appropriate choice over CD in very dense regimes of large numbers of particles because CD must solve, through iteration between each timestep, the contact forces between each particle in a contact chain. Still, HSDEM and CD can be a more appropriate collisional routine in more dilute regimes, where collisions do not involve networks consisting of large numbers of particles (e.g., higher energy, “granular gas” regimes; see Section 3 of this chapter), and where sound propagation speed is unimportant (the sound speed can be controlled in soft-sphere methodologies via a stiffness parameter). However, even in 2-body collisions, HSDEM can make errors. Particles can rotate significantly during realistic, finite, oblique collisions, altering the outcome of the collision—an effect that does not occur between perfectly rigid particles (Müller & Pöschel 2012). In addition to CD, attempts have been made to use HSDEM with added analytical corrections to account for rotations of the multi-body system while particles are colliding (Müller & Pöschel 2013), and to account for finite collision times (by “pausing” collisions). These are most effective in regimes when (third-) particle intruders can be safely ignored. Also, when two real (deformable) grains just “graze” each other, depending on the rigidity of the grains, they may interact very weakly; however, these types of contacts are given too much significance when using hard spheres (the assumption of grain incompressibility in HSDEM and CD leads to the exchange of too much energy and momentum during oblique impacts).

Despite these drawbacks, HSDEM and/or CD can be the appropriate choice in certain dilute/ballistic regimes (cf. Richardson *et al.* 2011; Murdoch *et al.* 2012), where they are advantageous over continuum models for their speed and accuracy, and often over SSDEM for their speed given the ability to handle large timesteps. These are regimes where collisional timescales may be long compared to other dynamical timescales (the “granular gas” regime; see Section 3 of this chapter), where contacts between grains do not persist and thus complex frictional forces are less relevant, and where the propagation of disturbance waves (material sound speeds) are unimportant.

For the simulation of dense environments, however, including many granular regimes in which grain deformation, finite sound speed, multicontact physics, and the complexity of higher-order frictional forces during contact cannot be neglected, SSDEM is the better choice. Although the use of small timesteps can limit its speed, it is well suited for true parallelisation (without the HSDEM drawback of having to compute collisions in serial order). Presently it is possible to follow the evolution of millions of grains in close contact and over a fairly large range of simulation conditions, something not possible with HSDEM.

The search for contacts in SSDEM is a simpler task than the search for contacts (collisions) in HSDEM. Before integrating over the next timestep, HSDEM must ask:

will there be a collision at any moment during the following timestep? In contrast, SSDEM needs only to ask if there are any overlaps presently occurring. Effectively, this means that contact searches are a 4-dimensional problem in HSDEM (3 spatial dimensions and 1 temporal dimension) and a 3-dimensional problem in SSDEM (3 spatial dimensions). More complex wall boundary geometries are more easily included in SSDEM (the SSDEM code implemented in `pkdgrav`, for example, allows for a wider set of wall boundaries; these include the triangle, which can allow for sophisticated 3-dimensional polyhedral shapes, along with those discussed in Schwartz *et al.* 2012).

As a direct comparison of the two DEM collisional methodologies, HSDEM and SSDEM, simulations of low-speed rubble pile collisions were performed using both SSDEM and HSDEM in the same numerical code (Richardson *et al.* 2012b). In the tests, self-gravitating rubble piles (without friction or cohesive forces) were collided together at low speed. The results from the two collisional routines were generally similar; SSDEM often, but not in all cases, showed a somewhat higher final ellipticity of the largest collisional remnant, suggesting a higher shear strength that may arise from its more careful treatment of contact forces and finite collisional times.

### 6.2.5. *The use of numerical simulation in the field of regolith dynamics*

Several DEM numerical codes have been written with the specific aim of investigating and solving for regolith dynamics. Walsh *et al.* (2008, 2012) used the HSDEM collisional routine in `pkdgrav` (Stadel 2001; Richardson *et al.* 2000) to study grain displacements and lofting due to YORP spinup. Soft-sphere collisional methodologies have been used to study regolith dynamics in low-gravity environments, which include subsonic impact cratering into regolith (Wada *et al.* 2006; Schwartz *et al.* 2014), the Brazil-nut effect (Tancredi *et al.* 2012; Matsumura *et al.* 2014), and regolith motion due to tidal forces (Yu *et al.* 2014). Also in the realm of asteroid surface science, several numerical investigations to study avalanche run-outs and angles of repose of regolith have been performed using both continuum codes (e.g., Holsapple 2013, using a finite-differencing method) and using DEM (e.g., Richardson *et al.* 2012a, using soft-sphere).

The inclusion of cohesion in numerical coding can be adapted to many different granular dynamics applications in planetary science, including the study of regolith dynamics (e.g., in SSDEM: Schwartz *et al.* 2013; Sánchez & Scheeres 2014). Attractive interparticle forces may be used to treat ionic or covalent molecular bonds, weaker intermolecular dipole-dipole bonds such as hydrogen bonds and London dispersion forces, or electrostatic forces.

## 7. CONCLUSIONS

In this chapter we have presented a brief overview of the observations of granular surfaces of asteroids, our current

understanding of the geophysical processes that may have occurred, and the state of the art experimental and computational methods used to study them and make new predictions. The field of regolith dynamics in varying gravitational environments, including the study of near-Earth asteroids as self-gravitating aggregates, is a new field of planetary science that will continue to evolve with the development of better computational tools and experimental techniques, refinements in the theoretical models and new in-situ observations from up-coming space missions such as OSIRIS-REx (NASA) and Hayabusa 2 (JAXA).

## 8. ACKNOWLEDGEMENTS

We would like to thank D. C. Richardson and D. J. Scheeres for their comments on our chapter and L. Staron and O. Barnouin for their very helpful reviews.

## REFERENCES

- Abe, S., Mukai, T., Hirata, N., et al. (2006) Mass and Local Topography Measurements of Itokawa by Hayabusa. *Science*, 312, 5778, 1344–1347.
- Alder, B. J. & Wainwright, T. E. (1959) Studies in Molecular Dynamics. I. General Method. *J. Chem. Phys.*, 31, 459–466.
- Andreotti, B., Forterre, Y., & Pouliquen, O. (2013) *Granular Media: Between Fluid and Solid*. Cambridge University Press. Cambridge Books Online.
- Asphaug, E. (2007) The Shifting Sands of Asteroids. *Science*, 316, 5827, 993–994.
- Asphaug, E. (2009) Growth and Evolution of Asteroids. *Ann. Rev. Earth Planet. Sci.*, 37, 1, 413–448.
- Asphaug, E. & Benz, W. (1994) Density of comet Shoemaker-Levy 9 deduced by modelling breakup of the parent ‘rubble pile’. *Nature*, 370, 120–124.
- Asphaug, E., King, P., Swift, M., & Merrifield, M. (2001) Brazil nuts on Eros: Size-sorting of Asteroid Regolith. In *Lunar and Planetary Science Conference*, 32, p. 1708.
- Asphaug, E., Moore, J. M., Morrison, D., et al. (1996) Mechanical and Geological Effects of Impact Cratering on Ida. *Icarus*, 120, 1, 158 – 184.
- Bagnold, R. (1966) The shearing and dilatation of dry sand and the ‘singing’ mechanism. *Proceedings of the Royal Society of London. Series A. Mathematical and Physical Sciences*, 295, 1442, 219–232.
- Bagnold, R. A. (1954) Experiments on a gravity-free dispersion of large solid spheres in a newtonian fluid under shear. *Proceedings of the Royal Society of London. Series A. Mathematical and Physical Sciences*, 225, 1160, 49–63.
- Barnouin-Jha, O. S., Cheng, A. F., Mukai, T., et al. (2008) Small-scale topography of 25143 Itokawa from the Hayabusa laser altimeter. *Icarus*, 198, 108–124.
- Barnouin-Jha, O. S., Garvin, J. B., Cheng, A. F., et al. (2001) Preliminary Impact Crater Dimensions on 433 Eros from the NEAR Laser Rangefinder and Imager. In *Lunar and Planetary Science Conference*, vol. 32 of *d*, p. 1786.
- Beitz, E., Güttler, C., Blum, J., et al. (2011) Low-velocity Collisions of Centimeter-sized Dust Aggregates. *The Astrophysical Journal*, 736, 34.
- Benz, W., Asphaug, E., & Ryan, E. V. (1994) Numerical simulations of catastrophic disruption: Recent results. *Planet. Space Sci.*, 42, 1053–1066.
- Bernu, B. & Mazighi, R. (1990) One-dimensional bounce of inelastically colliding marbles on a wall. *Journal of Physics A: Mathematical and General*, 23, 24, 5745.
- Besse, S., Kppers, M., Barnouin, O., et al. (2014) Lutetia’s lineaments. *Planetary and Space Science*, 101, 0, 186 – 195.
- Binzel, R. P., Morbidelli, A., Merouane, S., et al. (2010) Earth encounters as the origin of fresh surfaces on near-Earth asteroids. *Nature*, 463, 331–334.
- Biswas, P., Sánchez, P., Swift, M. R., & King, P. J. (2003) Numerical simulations of air-driven granular separation. *Phys. Rev. E*, 68, 050301.
- Bottke, W. F., Jr., Richardson, D. C., Michel, P., & Love, S. G. (1999) 1620 Geographos and 433 Eros: Shaped by Planetary Tides? *Astron. J.*, 117, 1921–1928.
- Bowden, F. & Leben, L. (1939) The nature of sliding and the analysis of friction. *Proceedings of the Royal Society of London. Series A, Mathematical and Physical Sciences*, pp. 371–391.
- Bowden, F. & Tabor, D. (1939) The area of contact between stationary and between moving surfaces. *Proceedings of the Royal Society of London. Series A, Mathematical and Physical Sciences*, pp. 391–413.
- Bowden, F. P., Moore, A. J. W., & Tabor, D. (1943) The ploughing and adhesion of sliding metals. *Journal of Applied Physics*, 14, 2, 80–91.
- Brahic, A. (1975) A numerical study of a gravitating system of colliding particles: Applications to the dynamics of saturn’s rings and to the formation of the solar system. *Icarus*, 25, 3, 452 – 458.
- Brahic, A. (1977) Systems of colliding bodies in a gravitational field. I-Numerical simulation of the standard model. *Astronomy and Astrophysics*, 54, 895–907.
- Bridgwater, J. (1976) Fundamental powder mixing mechanisms. *Powder Technology*, 15, 2, 215 – 236.
- Brilliantov, N. V. & Pöschel, T. (2010) *Kinetic theory of granular gases*. Oxford University Press.
- Buczkowski, D. L., Barnouin-Jha, O. S., & Prockter, L. M. (2008) 433 Eros lineaments: Global mapping and analysis. *Icarus*, 193, 39–52.
- Burtally, N., King, P. J., & Swift, M. R. (2002) Spontaneous air-driven separation in vertically vibrated fine granular mixtures. *Science*, 295, 5561, 1877–1879.
- Carr, M. H., Kirk, R. L., McEwen, A., et al. (1994) The geology of Gaspra. *Icarus*, 107, 61.
- Carrigy, M. A. (1970) Experiments on the angles of repose of granular materials. *Sedimentology*, 14, 3-4, 147–158.

- Cassidy, T. & Johnson, R. (2005) Monte carlo model of sputtering and other ejection processes within a regolith. *Icarus*, 176, 2, 499 – 507.
- Castellanos, A. (2005) The relationship between attractive interparticle forces and bulk behaviour in dry and uncharged fine powders. *Advances in Physics*, 54, 4, 263–376.
- Chapman, C. R. (1976) Asteroids as meteorite parent bodies - The astronomical perspective. *Geochimica et Cosmochimica Acta*, 40, 701–719.
- Chapman, C. R. (2004) Space weathering of asteroid surfaces. *Annual Review of Earth and Planetary Sciences*, 32, 1, 539–567.
- Chen, W. & Han, D. (1988) Plasticity for structural engineers. *Springer, New York*.
- Cheng, A. F. (2002) Near Earth Asteroid Rendezvous: Mission Summary. *Asteroids III*, pp. 351–366.
- Cheng, A. F., Barnouin-Jha, O., Hirata, N., et al. (2007) Fundamentally distinct outcomes of asteroid collisional evolution: Itokawa and Eros. *Geophys. Res. Lett.*, 34, L09201.
- Cheng, A. F., Barnouin-Jha, O., Prockter, L., et al. (2002a) Small-Scale Topography of 433 Eros from Laser Altimetry and Imaging. *Icarus*, 155, 51–74.
- Cheng, A. F., Izenberg, N., Chapman, C. R., & Zuber, M. T. (2002b) Ponded deposits on asteroid 433 Eros. *Meteoritics and Planetary Science*, 37, 1095–1105.
- Cheng, A. F., Santo, A. G., Heeres, K. J., et al. (1997) Near-Earth Asteroid Rendezvous: mission overview. *J. Geophys. Res.*, 102, 23695–23708.
- Chladni, E. (1787) *Entdeckungen über die theorie des klages*. Bey Weidmanns erben und Reich.
- Cleary, P. W. & Sawley, M. L. (2002) DEM modelling of industrial granular flows: 3D case studies and the effect of particle shape on hopper discharge. *Appl. Math. Modell.*, 26, 89–111.
- Colwell, J. E. (2003) Low velocity impacts into dust: results from the COLLIDE-2 microgravity experiment. *Icarus*, 164, 188–196.
- Colwell, J. E., Gulbis, A. A., Horányi, M., & Robertson, S. (2005) Dust transport in photoelectron layers and the formation of dust ponds on Eros. *Icarus*, 175, 1, 159 – 169.
- Coradini, A., Capaccioni, F., Erard, S., et al. (2011) The Surface Composition and Temperature of Asteroid 21 Lutetia As Observed by Rosetta/VIRTIS. *Science*, 334, 492–.
- Costantino, D. J., Scheidemantel, T. J., Stone, M. B., et al. (2008) Starting to Move through a Granular Medium. *Phys. Rev. Lett.*, 101, 108001.
- Coulomb, C. A. (1776) *Essai sur une application des règles de maximis & minimis à quelques problèmes de statique, relatifs à l'architecture*. De l'Imprimerie Royale, Paris.
- Crosta, G. B., Imposimato, S., & Roddeman, D. (2009) Numerical modeling of 2-d granular step collapse on erodible and nonerodible surface. *Journal of Geophysical Research: Earth Surface*, 114, F3.
- Cundall, P. A. & Strack, O. D. L. (1979) A discrete numerical model for granular assemblies. *Géotechnique*, 29, 47–65.
- de Gennes, P. G. (1999) Granular matter: a tentative view. *Rev. Mod. Phys.*, 71, S374–S382.
- Delbo, M., Libourel, G., Wilkerson, J., et al. (2014) Thermal fatigue as the origin of regolith on small asteroids. *Nature*, 508, 233–236.
- Demura, H., Kobayashi, S., Nemoto, E., et al. (2006) Pole and global shape of 25143 Itokawa. *Science*, 312, 5778, 1347–1349.
- Denevi, B. W., Blewett, D. T., Buczowski, D. L., et al. (2012) Pitted Terrain on Vesta and Implications for the Presence of Volatiles. *Science*, 338, 246–.
- Dollfus, A., Geake, J. E., Mandeville, J. C., & Zellner, B. (1977) The nature of asteroid surfaces, from optical polarimetry. In A. H. Delsemme, ed., *IAU Colloq. 39: Comets, Asteroids, Meteorites: Interrelations, Evolution and Origins*, pp. 243–251.
- Dombard, A. J., Barnouin, O. S., Prockter, L. M., & Thomas, P. C. (2010) Boulders and ponds on the Asteroid 433 Eros. *Icarus*, 210, 2, 713 – 721.
- Dombard, A. J. & Freed, A. M. (2002) Thermally induced lineations on the asteroid Eros: Evidence of orbit transfer. *Geophys. Res. Lett.*, 29, 16.
- Dove, A. & Colwell, J. E. (2013) Investigations of charged particle motion on the surfaces of dusty, airless solar system bodies (Invited). *AGU Fall Meeting Abstracts*, p. F1.
- Durda, D., Devaud, G., Scheeres, D., et al. (2013) Laboratory investigation of asteroid regolith properties. In *EPSC 2013 Proceedings*.
- Elaskar, S. A., Godoy, L. A., Gray, D. D., & Stiles, J. M. (2000) A viscoplastic approach to model the flow of granular solids. *Int. J. Solids Struct.*, 37, 2185–2214.
- Fall, A., Weber, B., Pakpour, M., et al. (2014) Sliding friction on wet and dry sand. *Phys. Rev. Lett.*, 112, 175502.
- Faraday, M. (1831) On a peculiar class of acoustical figures; and on certain forms assumed by groups of particles upon vibrating elastic surfaces. *Philosophical Transactions of the Royal Society of London*, 121, pp. 299–340.
- Forterre, Y. & Pouliquen, O. (2008) Flows of Dense Granular Media. *Annual Review of Fluid Mechanics*, 40, 1, 1–24.
- Fu, H., Jedicke, R., Durda, D. D., et al. (2005) Identifying near-Earth object families. *Icarus*, 178, 434–449.
- Fujiwara, A. & Asada, N. (1983) Impact fracture patterns on phobos ellipsoids. *Icarus*, 56, 3, 590 – 602.
- Fujiwara, A., Kawaguchi, J., Yeomans, D. K., et al. (2006) The Rubble-Pile Asteroid Itokawa as Observed by Hayabusa. *Science*, 312, 5778, 1330–1334.
- GDR-MiDi (2004) On dense granular flows. *The European Physical Journal E*, 14, 4, 341–365.
- Geissler, P., Petit, J. M., & Greenberg, R. (1996) Ejecta Reaccretion on Rapidly Rotating Asteroids: Implications for 243 Ida and 433 Eros. In T. Rettig & J. M. Hahn, eds., *Completing the Inventory of the Solar System*, vol.

- 107 of *Astronomical Society of the Pacific Conference Series*, pp. 57–67.
- Gray, J. M. N. T. & Chugunov, V. A. (2006) Particle-size segregation and diffusive remixing in shallow granular avalanches. *Journal of Fluid Mechanics*, 569, 365–398.
- Gudhe, R., Yalamanchili, R., & Massoudi, M. (1994) Flow of granular materials down a vertical pipe. *International Journal of Non-Linear Mechanics*, 29, 1, 1 – 12.
- Güttler, C., von Borstel, I., Schräpler, R., & Blum, J. (2013) Granular convection and the brazil nut effect in reduced gravity. *Phys. Rev. E*, 87, 044201.
- Haff, P. (1983) Grain flow as a fluid-mechanical phenomenon. *Journal of Fluid Mechanics*, 134, 1, 401–430.
- Hapke, B. & van Hoen, H. (1963) Photometric studies of complex surfaces, with applications to the moon. *Journal of Geophysical Research*, 68, 15, 4545–4570.
- Harris, A. W. (2006) The surface properties of small asteroids from thermal-infrared observations. In L. Daniela, M. Sylvio Ferraz, & F. J. Angel, eds., *Asteroids, Comets, Meteors*, vol. 229 of *IAU Symposium*, pp. 449–463.
- Harris, A. W., Fahnstock, E. G., & Pravec, P. (2009) On the shapes and spins of “rubble pile” asteroids. *Icarus*, 199, 310–318.
- Hartzell, C., Wang, X., Scheeres, D., & Horányi, M. (2013) Experimental demonstration of the role of cohesion in electrostatic dust lofting. *Geophys. Res. Lett.*, 40, 6, 1038–1042.
- Hartzell, C. M. & Scheeres, D. J. (2011) The role of cohesive forces in particle launching on the moon and asteroids. *Planetary and Space Science*, 59, 14, 1758 – 1768. Lunar Dust, Atmosphere and Plasma: The Next Steps.
- Hartzell, C. M. & Scheeres, D. J. (2013) Dynamics of levitating dust particles near asteroids and the Moon. *Journal of Geophysical Research: Planets*, 118, 1, 116–125.
- Heim, L.-O., Blum, J., Preuss, M., & Butt, H.-J. (1999) Adhesion and friction forces between spherical micrometer-sized particles. *Phys. Rev. Lett.*, 83, 3328–3331.
- Herrick, R. R. & Hessen, K. K. (2006) The planforms of low-angle impact craters in the northern hemisphere of Mars. *Meteoritics and Planetary Science*, 41, 1483–1495.
- Hirabayashi, M. (2014) Structural failure of two-density-layer cohesionless biaxial ellipsoids. *Icarus*, 236, 0, 178 – 180.
- Hirabayashi, M., Scheeres, D. J., Sánchez, D. P., & Gabriel, T. (2014) Constraints on the physical properties of main belt comet p/2013 r3 from its breakup event. *The Astrophysical Journal Letters*, 789, 1, L12.
- Hoerz, F., Schneider, E., Gault, D. E., et al. (1975) Catastrophic rupture of lunar rocks - A Monte Carlo simulation. *Moon*, 13, 235–258.
- Hofmeister, P. G., Blum, J., & Heißelmann, D. (2009) The flow of granular matter under reduced-gravity conditions. *AIP Conference Proceedings*, 1145, 1, 71–74.
- Holsapple, K. A. (1993) The scaling of impact processes in planetary sciences. *Annual Review of Earth and Planetary Sciences*, 21, 333–373.
- Holsapple, K. A. (2004) Equilibrium figures of spinning bodies with self-gravity. *Icarus*, 172, 272–303.
- Holsapple, K. A. (2009) On the “strength” of the small bodies of the solar system: A review of strength theories and their implementation for analyses of impact disruptions. *Planet. Space Sci.*, 57, 127–141.
- Holsapple, K. A. (2013) Modeling granular material flows: The angle of repose, fluidization and the cliff collapse problem. *Planet. Space Sci.*, 82–83, 0, 11 – 26.
- Holsapple, K. A. & Michel, P. (2006) Tidal disruptions: A continuum theory for solid bodies. *Icarus*, 183, 331–348.
- Holsapple, K. A. & Michel, P. (2008) Tidal disruptions. II. A continuum theory for solid bodies with strength, with applications to the Solar System. *Icarus*, 193, 283–301.
- Housen, K. R. & Holsapple, K. A. (2011) Ejecta from impact craters. *Icarus*, 211, 856–875.
- Housen, K. R., Wilkening, L. L., Chapman, C. R., & Greenberg, R. (1979) Asteroidal regoliths. *Icarus*, 39, 317–351.
- Hughes, A. L., Colwell, J. E., & DeWolfe, A. W. (2008) Electrostatic dust transport on Eros: 3-D simulations of pond formation. *Icarus*, 195, 2, 630 – 648.
- Jaeger, H. M., Nagel, S. R., & Behringer, R. P. (1996) Granular solids, liquids, and gases. *Rev. Mod. Phys.*, 68, 1259–1273.
- Janssen, H. A. (1895) Versuche über Getreidedruck in Silozellen. *Zeitschr. d. Vereines deutscher Ingenieure*, 39, 35, 1045–1049.
- Jaumann, R., Nass, A., Otto, K., et al. (2014) The geological nature of dark material on vesta and implicatons for the subsurface structure. *Icarus*, , 0, –.
- Jaumann, R., Williams, D. A., Buczkowski, D. L., et al. (2012) Vesta’s Shape and Morphology. *Science*, 336, 687–.
- Jenkins, J. T. & Zhang, C. (2002) Kinetic theory for identical, frictional, nearly elastic spheres. *Physics of Fluids (1994-present)*, 14, 3, 1228–1235.
- Jewitt, D. (2012) The Active Asteroids. *The Astronomical Journal*, 143, 66.
- Johnson, K. L., Kendall, K., & Roberts, A. D. (1971) Surface energy and the contact of elastic solids. *Proceedings of the Royal Society of London. A. Mathematical and Physical Sciences*, 324, 1558, 301–313.
- Jones, J. E. (1924) On the determination of molecular fields. i. from the variation of the viscosity of a gas with temperature. *Proceedings of the Royal Society of London. Series A*, 106, 738, 441–462.
- Jop, P., Forterre, Y., & Pouliquen, O. (2006) A constitutive law for dense granular flows. *Nature*, 441, 727–730.
- Jutzi, M. & Asphaug, E. (2011) Mega-ejecta on asteroid Vesta. *Geophys. Res. Lett.*, 38, L01102.
- Jutzi, M., Asphaug, E., Gillet, P., et al. (2013) The structure of the asteroid 4Vesta as revealed by models of planet-scale collisions. *Nature*, 494, 207–210.

- Keller, H. U., Barbieri, C., Koschny, D., et al. (2010) E-Type Asteroid (2867) Steins as Imaged by OSIRIS on Board Rosetta. *Science*, 327, 190–.
- Kleinbans, M. G., Markies, H., de Vet, S. J., et al. (2011) Static and dynamic angles of repose in loose granular materials under reduced gravity. *Journal of Geophysical Research: Planets*, 116, E11, n/a–n/a.
- Knight, J. B., Jaeger, H. M., & Nagel, S. R. (1993) Vibration-induced size separation in granular media: The convection connection. *Phys. Rev. Lett.*, 70, 24, 3728–3731.
- Kosinski, P. & Hoffmann, A. C. (2009) Extension of the hard-sphere particle-wall collision model to account for particle deposition. *Phys. Rev. E*, 79, 6, 061302.
- Krause, M. & Blum, J. (2004) Growth and Form of Planetary Seedlings: Results from a Sounding Rocket Microgravity Aggregation Experiment. *Physical Review Letters*, 93, 2, 021103.
- Kreslavsky, M. A. & Shkuratov, Y. G. (2003) Photometric anomalies of the lunar surface: Results from clementine data. *Journal of Geophysical Research: Planets*, 108, E3, n/a–n/a.
- Krohn, K., Jaumann, R., Elbeshausen, D., et al. (2014) Asymmetric craters on vesta: Impact on sloping surfaces. *Planet. Space Sci.*, 0, –.
- Kudrolli, A. (2004) Size separation in vibrated granular matter. *Reports on Progress in Physics*, 67, 3, 209.
- Küppers, M., Moissl, R., Vincent, J.-B., et al. (2012) Boulders on Lutetia. *Planet. Space Sci.*, 66, 71–78.
- Lagrée, P.-Y., Staron, L., & Popinet, S. (2011) The granular column collapse as a continuum: validity of a two-dimensional navier–stokes model with a  $\mu$  (i)-rheology. *Journal of Fluid Mechanics*, 686, 378–408.
- Lamy, P. L., Faury, G., Jorda, L., et al. (2010) Multi-color, rotationally resolved photometry of asteroid 21 Lutetia from OSIRIS/Rosetta observations. *Astron. Astrophys.*, 521, A19.
- Lee, P. (1996) Dust Levitation on Asteroids. *Icarus*, 124, 181–194.
- Legros, F. (2002) The mobility of long-runout landslides. *Engineering Geology*, 63, 34, 301 – 331.
- Luding, S. & McNamara, S. (1998) How to handle the inelastic collapse of a dissipative hard-sphere gas with the tc model. *Granular Matter*, 1, 3, 113–128.
- Mantz, A., Sullivan, R., & Veverka, J. (2004) Regolith transport in craters on Eros. *Icarus*, 167, 197–203.
- Marchi, S., McSween, H. Y., O’Brien, D. P., et al. (2012) The Violent Collisional History of Asteroid 4 Vesta. *Science*, 336, 690–.
- Martí, M. & Mulet, P. (2014) Some techniques for improving the resolution of finite difference component-wise weno schemes for polydisperse sedimentation models. *Applied Numerical Mathematics*, 78, 1–13.
- Massironi, M., Marchi, S., Pajola, M., et al. (2012) Geological map and stratigraphy of asteroid 21 Lutetia. *Planet. Space Sci.*, 66, 125–136.
- Matson, D. L. & Nash, D. B. (1983) Io’s atmosphere: Pressure control by regolith cold trapping and surface venting. *Journal of Geophysical Research: Space Physics*, 88, A6, 4771–4783.
- Matsumura, S., Richardson, D. C., Michel, P., et al. (2014) The Brazil nut effect and its application to asteroids. *Mon. Not. R. Astron. Soc.*, 443, 3368–3380.
- Mazrouei, S., Daly, M., Barnouin, O., et al. (2012) Distribution of Boulders on Asteroid 25143 Itokawa. In *Lunar and Planetary Science Conference*, vol. 43, p. 2404.
- McCarthy, J. J. (2009) Turning the corner in segregation. *Powder Technology*, 192, 2, 137 – 142.
- McGetchin, T., Settle, M., & Head, J. (1973) Radial thickness variation in impact crater ejecta: implications for lunar basin deposits. *Earth and Planetary Science Letters*, 20, 2, 226 – 236.
- McNamara, S. (2000) Inelastic collapse. In J. Karkheck, ed., *Dynamics: Models and Kinetic Methods for Non-equilibrium Many Body Systems*, pp. 267–277. Kluwer, Dordrecht.
- McNamara, S. & Young, W. R. (1992) Inelastic collapse and clumping in a one-dimensional granular medium. *Physics of Fluids A*, 4, 496–504.
- McNaught, A. D. & Wilkinson, A. (1997) *IUPAC. Compendium of chemical terminology*, vol. 1669. Blackwell Science Oxford. XML on-line corrected version.
- McSween, H. Y., Mittlefehldt, D. W., Beck, A. W., et al. (2011) HED Meteorites and Their Relationship to the Geology of Vesta and the Dawn Mission. *Space Science Reviews*, 163, 141–174.
- Mehta, A. (2007) *Granular physics*. Cambridge University Press.
- Melosh, H. J. (1989) *Impact cratering: A geologic process*. Oxford Monographs on Geology and Geophysics.
- Mériaux, C. & Triantafyllou, T. (2008) Scaling the final deposits of dry cohesive granular columns after collapse and quasi-static fall. *Physics of Fluids (1994-present)*, 20, 3, 033301.
- Meunier, P., Uchida, T., & Hovius, N. (2013) Landslide patterns reveal the sources of large earthquakes. *Earth and Planetary Science Letters*, 363, 0, 27 – 33.
- Michel, P., Benz, W., Tanga, P., & Richardson, D. C. (2001) Collisions and Gravitational Reaccumulation: Forming Asteroid Families and Satellites. *Science*, 294, 1696–1700.
- Michel, P., O’Brien, D. P., Abe, S., & Hirata, N. (2009) Itokawa’s cratering record as observed by Hayabusa: Implications for its age and collisional history. *Icarus*, 200, 503–513.
- Michikami, T., Nakamura, A. M., Hirata, N., et al. (2008) Size-frequency statistics of boulders on global surface of asteroid 25143 Itokawa. *Earth, Planets, and Space*, 60, 13–20.
- Miller, J. K., Konopliv, A. S., Antreasian, P. G., et al. (2002) Determination of Shape, Gravity, and Rotational State of Asteroid 433 Eros. *Icarus*, 155, 3–17.

- Miyamoto, H. (2014) Unconsolidated boulders on the surface of Itokawa. *Planet. Space Sci.*, 95, 94–102.
- Miyamoto, H., Yano, H., Scheeres, D. J., et al. (2007) Regolith Migration and Sorting on Asteroid Itokawa. *Science*, 316, 5827, 1011–1014.
- Monaghan, J. J. (1988) An introduction to SPH. *Computer physics communications*, 48, 1, 89–96.
- Moreau, J. J. (1994) Some numerical methods in multibody dynamics: application to granular materials. *European journal of mechanics. A. Solids*, 13, 93–114.
- Müller, P. & Pöschel, T. (2012) Oblique impact of frictionless spheres: on the limitations of hard sphere models for granular dynamics. *Granular Matter*, 14, 2, 115–120.
- Müller, P. & Pöschel, T. (2013) Event-driven molecular dynamics of soft particles. *Physical Review E*, 87, 3, 033301.
- Murchie, S., Robinson, M., Clark, B., et al. (2002) Color Variations on Eros from NEAR Multispectral Imaging. *Icarus*, 155, 145–168.
- Murdoch, N., Michel, P., Richardson, D. C., et al. (2012) Numerical simulations of granular dynamics II. Particle dynamics in a shaken granular material. *Icarus*, 219, 1, 231–335.
- Murdoch, N., Rozitis, B., Green, S., et al. (2013a) Granular shear flow in varying gravitational environments. *Granular Matter*, 15, 2, 129–137.
- Murdoch, N., Rozitis, B., Green, S. F., et al. (2013b) Simulating regoliths in microgravity. *Mon. Not. R. Astron. Soc.*
- Murdoch, N., Rozitis, B., Nordstrom, K., et al. (2013c) Granular Convection in Microgravity. *Phys. Rev. Lett.*, 110, 018307.
- Nakamura, A. M., Fujiwara, A., & Kadono, T. (1994) Velocity of finer fragments from impact. *Planet. Space Sci.*, 42, 1043–1052.
- Nakamura, T., Noguchi, T., Tanaka, M., et al. (2011) Itokawa Dust Particles: A Direct Link Between S-Type Asteroids and Ordinary Chondrites. *Science*, 333, 1113.
- Nedderman, R. M. (2005) *Statics and kinematics of granular materials*. Cambridge University Press.
- Nesvorný, D., Bottke, W. F., Vokrouhlický, D., et al. (2010) Do planetary encounters reset surfaces of near Earth asteroids? *Icarus*, 209, 510–519.
- Nichol, K., Zanin, A., Bastien, R., et al. (2010) Flow-Induced Agitations Create a Granular Fluid. *Phys. Rev. Lett.*, 104, 078302.
- Perko, H., Nelson, J., & Sadeh, W. (2001) Surface cleanliness effect on lunar soil shear strength. *Journal of Geotechnical and Geoenvironmental Engineering*, 127, 4, 371–383.
- Petit, J.-M. & Henon, M. (1987) A numerical simulation of planetary rings. I - Binary encounters. *Astron. Astrophys.*, 173, 389–404.
- Pieters, C. M., Ammannito, E., Blewett, D. T., et al. (2012) Distinctive space weathering on Vesta from regolith mixing processes. *Nature*, 491, 79–82.
- Pohlman, N. A., Severson, B. L., Ottino, J. M., & Lueptow, R. M. (2006) Surface roughness effects in granular matter: Influence on angle of repose and the absence of segregation. *Phys. Rev. E*, 73, 031304.
- Pravec, P., Vokrouhlický, D., Polishook, D., et al. (2010) Formation of asteroid pairs by rotational fission. *Nature*, 466, 1085–1088.
- Prockter, L., Thomas, P., Robinson, M., et al. (2002) Surface Expressions of Structural Features on Eros. *Icarus*, 155, 1, 75 – 93.
- Radjai, F. & Dubois, F. (2011) *Discrete-element modeling of granular materials*. Berlin: Wiley-ISTE.
- Rao, K. K., Nott, P. R., & Sundaresan, S. (2008) *An introduction to granular flow*. Cambridge University Press New York.
- Rennilson, J. & Criswell, D. (1974) Surveyor observations of lunar horizon-glow. *The Moon*, 10, 2, 121–142.
- Richard, P., Nicodemi, M., Delannay, R., et al. (2005) Slow relaxation and compaction of granular systems. *Nature Materials*, 4, 121–128.
- Richardson, D. C. (1994) Tree Code Simulations of Planetary Rings. *Mon. Not. R. Astron. Soc.*, 269, 493.
- Richardson, D. C. (1995) A Self-Consistent Numerical Treatment of Fractal Aggregate Dynamics. *Icarus*, 115, 320–335.
- Richardson, D. C., Blum, J., Weinhart, T., et al. (2012a) Numerical Simulations of Landslides Calibrated Against Laboratory Experiments for Application to Asteroid Surface Processes. In *AAS/Division for Planetary Sciences Meeting Abstracts #44*, vol. 44 of *AAS/Division for Planetary Sciences Meeting Abstracts #44*, p. #105.06.
- Richardson, D. C., Bottke, W. F., & Love, S. G. (1998) Tidal Distortion and Disruption of Earth-Crossing Asteroids. *Icarus*, 134, 47–76.
- Richardson, D. C., Leinhardt, Z. M., Melosh, H. J., et al. (2002) Gravitational Aggregates: Evidence and Evolution. *Asteroids III*, pp. 501–515.
- Richardson, D. C., Munyan, S. K., Schwartz, S. R., & Michel, P. (2012b) Comparison of Discrete Element Methods for Simulating Low-Speed Rubble Pile Collisions: First Results. In *Lunar and Planetary Science Conference*, vol. 43 of *Lunar and Planetary Inst. Technical Report*, p. 2195.
- Richardson, D. C., Quinn, T., Stadel, J., & Lake, G. (2000) Direct Large-Scale N-Body Simulations of Planetesimal Dynamics. *Icarus*, 143, 45–59.
- Richardson, D. C., Walsh, K. J., Murdoch, N., & Michel, P. (2011) Numerical simulations of granular dynamics: I. Hard-sphere discrete element method and tests. *Icarus*, 212, 427–437.
- Richardson, J. E., Jr., Melosh, H. J., et al. (2005) The global effects of impact-induced seismic activity on fractured asteroid surface morphology. *Icarus*, 179, 2, 325 – 349.
- Richardson, J. E., Melosh, H. J., & Greenberg, R. (2004) Impact-Induced Seismic Activity on Asteroid 433 Eros: A Surface Modification Process. *Science*, 306, 5701, 1526–1529.

- Riner, M. A., Robinson, M. S., Eckart, J. M., & Desch, S. J. (2008) Global survey of color variations on 433 Eros: Implications for regolith processes and asteroid environments. *Icarus*, 198, 67–76.
- Roberts, J., Kahn, E., Barnouin, O., et al. (2014a) Not all ponds are flat: A stereophotoclinometric analysis of topography on 433 Eros. *Meteorit. Planet. Sci.*, *In Press*.
- Roberts, J. H., Barnouin, O. S., Kahn, E. G., & Prockter, L. M. (2014b) Observational bias and the apparent distribution of ponds on Eros. *Icarus*, 241, 0, 160–164.
- Robinson, M. S., Thomas, P. C., Veverka, J., et al. (2001) The nature of ponded deposits on Eros. *Nature*, 413, 6854, 396–400.
- Robinson, M. S., Thomas, P. C., Veverka, J., et al. (2002) The geology of 433 Eros. *Meteoritics and Planetary Science*, 37, 1651–1684.
- Rognon, P. G., Roux, J.-N., NaaIM, M., & Chevoir, F. (2008) Dense flows of cohesive granular materials. *Journal of Fluid Mechanics*, 596, 21–47.
- Rosato, A., Strandburg, K. J., Prinz, F., & Swendsen, R. H. (1987) Why the Brazil nuts are on top: Size segregation of particulate matter by shaking. *Phys. Rev. Lett.*, 58, 10, 1038–1040.
- Rozitis, B., MacLennan, E., & Emery, J. P. (2014) Cohesive forces prevent the rotational breakup of rubble-pile asteroid (29075) 1950 da. *Nature*, 512, 7513, 174–176.
- Russell, C. T. & Raymond, C. A. (2011) The Dawn Mission to Vesta and Ceres. *Space Science Reviews*, 163, 3–23.
- Russell, C. T., Raymond, C. A., Coradini, A., et al. (2012) Dawn at Vesta: Testing the Protoplanetary Paradigm. *Science*, 336, 684–.
- Saito, J., Miyamoto, H., Nakamura, R., et al. (2006) Detailed Images of Asteroid 25143 Itokawa from Hayabusa. *Science*, 312, 5778, 1341–1344.
- Sánchez, P. & Scheeres, D. J. (2011) Simulating Asteroid Rubble Piles with A Self-gravitating Soft-sphere Distinct Element Method Model. *Astrophys. J.*, 727, 120.
- Sánchez, P. & Scheeres, D. J. (2014) The strength of regolith and rubble pile asteroids. *Meteoritics and Planetary Science*, 49, 788–811.
- Scheeres, D., Gaskell, R., Abe, S., et al. (2006) The Actual Dynamical Environment About Itokawa. In *AIAA/AAS Astrodynamics Specialist Conference and Exhibit*. American Institute of Aeronautics and Astronautics.
- Scheeres, D., Hartzell, C., Sánchez, P., & Swift, M. (2010) Scaling forces to asteroid surfaces: The role of cohesion. *Icarus*, 210, 2, 968–984.
- Scheeres, D. J. (2005) Solar Radiation Pressure and Transient Flows on Asteroid Surfaces. In S. Mackwell & E. Stansbery, eds., *Lunar and Planetary Science Conference*, vol. 36, p. 1919.
- Scheeres, D. J. (2014) Solar system: Sandcastles in space. *Nature*, 512, 7513, 139–140.
- Scheeres, D. J., Abe, M., Yoshikawa, M., et al. (2007) The effect of YORP on Itokawa. *Icarus*, 188, 425–429.
- Schräpler, R., Blum, J., Seizinger, A., & Kley, W. (2012) The Physics of Protoplanetary Dust Agglomerates. VII. The Low-velocity Collision Behavior of Large Dust Agglomerates. *The Astrophysical Journal*, 758, 35.
- Schroter, M., Goldman, D. I., & Swinney, H. L. (2005) Stationary state volume fluctuations in a granular medium. *Phys. Rev. E*, 71, 3, 030301.
- Schulz, R., Sierks, H., Küppers, M., & Accomazzo, A. (2012) Rosetta fly-by at asteroid (21) Lutetia: An overview. *Planet. Space Sci.*, 66, 2–8.
- Schwartz, S. R., Michel, P., & Richardson, D. C. (2013) Numerically simulating impact disruptions of cohesive glass bead agglomerates using the soft-sphere discrete element method. *Icarus*, 226, 67–76.
- Schwartz, S. R., Michel, P., Richardson, D. C., & Yano, H. (2014) Low-speed impact simulations into regolith in support of asteroid sampling mechanism design i.: Comparison with 1-g experiments. *Planet. Space Sci.*
- Schwartz, S. R., Richardson, D. C., & Michel, P. (2012) An implementation of the soft-sphere discrete element method in a high-performance parallel gravity tree-code. *Granular Matter*, 14, 363–380.
- Sharma, I., Jenkins, J. T., & Burns, J. A. (2009) Dynamical passage to approximate equilibrium shapes for spinning, gravitating rubble asteroids. *Icarus*, 200, 304–322.
- Shoemaker, E. M., Batson, R. M., Holt, H. E., et al. (1968) Television Observations from Surveyor 3. *J. Geophys. Res.*, 73, 3989.
- Sierks, H., Lamy, P., Barbieri, C., et al. (2011) Images of Asteroid 21 Lutetia: A Remnant Planetesimal from the Early Solar System. *Science*, 334, 487–.
- Sirono, S.-I. (2004) Conditions for collisional growth of a grain aggregate. *Icarus*, 167, 431–452.
- Springel, V. (2010) Smoothed particle hydrodynamics in astrophysics. *Annual Review of Astronomy and Astrophysics*, 48, 1, 391–430.
- Springel, V. & Hernquist, L. (2002) Cosmological smoothed particle hydrodynamics simulations: the entropy equation. *Mon. Not. R. Astron. Soc.*, 333, 3, 649–664.
- Stadel, J. G. (2001) Cosmological N-body simulations and their analysis. Ph.D. thesis, University of Washington.
- Sullivan, R., Greeley, R., Pappalardo, R., et al. (1996) Geology of 243 Ida. *Icarus*, 120, 119–139.
- Sullivan, R. J., Thomas, P. C., Murchie, S. L., & Robinson, M. S. (2002) Asteroid Geology from Galileo and NEAR Shoemaker Data. *Asteroids III*, pp. 331–350.
- Tancredi, G., Maciel, A., Heredia, L., et al. (2012) Granular physics in low-gravity environments using discrete element method. *Mon. Not. R. Astron. Soc.*, 420, 3368–3380.
- Taylor, G. J. (1993) Rapid Magma Migration in Asteroids. *Meteoritics*, 28, 447–448.
- Thomas, N., Barbieri, C., Keller, H. U., et al. (2012) The geomorphology of (21) Lutetia: Results from the OSIRIS imaging system onboard ESA’s Rosetta spacecraft. *Planetary and Space Science*, 66, 96–124.

- Thomas, P., Veverka, J., Bloom, A., & Duxbury, T. (1979) Grooves on Phobos: Their Distribution, Morphology and Possible Origin. *J. Geophys. Res.*, *84*, B14, 8457–8477.
- Thomas, P. C., A’Hearn, M. F., Veverka, J., et al. (2013) Shape, density, and geology of the nucleus of Comet 103P/Hartley 2. *Icarus*, *222*, 550–558.
- Thomas, P. C., Joseph, J., Carcich, B., et al. (2002) Eros: Shape, Topography, and Slope Processes. *Icarus*, *155*, 18–37.
- Thomas, P. C. & Robinson, M. S. (2005) Seismic resurfacing by a single impact on the asteroid 433 Eros. *Nature*, *436*, 366–369.
- Thomas, P. C., Veverka, J., Bell, J. F., et al. (1999) Mathilde: Size, Shape, and Geology. *Icarus*, *140*, 17–27.
- Thomas, P. C., Veverka, J., Robinson, M. S., & Murchie, S. (2001) Shoemaker crater as the source of most ejecta blocks on the asteroid 433 Eros. *Nature*, *413*, 394–396.
- Thomas, P. C., Veverka, J., Sullivan, R., et al. (2000) Phobos: Regolith and ejecta blocks investigated with Mars Orbiter Camera images. *Journal of Geophysical Research*, *105*, 15091–15106.
- Thornton, A. (2005) A study of segregation in granular gravity driven free surface flows. Ph.D. thesis, The University of Manchester.
- Tsuchiyama, A., Uesugi, M., Matsushima, T., et al. (2011) Three-Dimensional Structure of Hayabusa Samples: Origin and Evolution of Itokawa Regolith. *Science*, *333*, 6046, 1125–1128.
- Tsuji, Y., Tanaka, T., & T., I. (1992) Lagrangian numerical simulation of plug flow of cohesionless particles in a horizontal pipe. *Powder Technol.*, *71*, 239–250.
- Veverka, J., Farquhar, B., Robinson, M., et al. (2001) The landing of the NEAR-Shoemaker spacecraft on asteroid 433 Eros. *Nature*, *413*, 390–393.
- Veverka, J., Farquhar, B., Robinson, M., et al. (2001) The landing of the NEAR-Shoemaker spacecraft on asteroid 433 Eros.
- Veverka, J., Klaasen, K., A’Hearn, M., et al. (2013) Return to comet tempel 1: Overview of stardust-next results. *Icarus*, *222*, 2, 424 – 435. Stardust/EPOXI.
- Veverka, J., Robinson, M., Thomas, P., et al. (2000) NEAR at Eros: Imaging and Spectral Results. *Science*, *289*, 5487, 2088–2097.
- Veverka, J., Thomas, P. C., Robinson, M., et al. (2001) Imaging of Small-Scale Features on 433 Eros from NEAR: Evidence for a Complex Regolith. *Science*, *292*, 484–488.
- Vincent, J.-B., Besse, S., Marchi, S., et al. (2012) Physical properties of craters on asteroid (21) Lutetia. *Planet. Space Sci.*, *66*, 79–86.
- Vincent, J.-B., Schenk, P., Nathues, A., et al. (2013) Crater depth-to-diameter distribution and surface properties of (4) vesta. *Planet. Space Sci.*, *0*, –.
- Vokrouhlický, D., Nesvorný, D., & Bottke, W. F. (2003) The vector alignments of asteroid spins by thermal torques. *Nature*, *425*, 147–151.
- von Neumann, J. & Richtmyer, R. D. (1950) A method for the numerical calculation of hydrodynamic shocks. *Journal of Applied Physics*, *21*, 3, 232–237.
- Wada, K., Senshu, H., & Matsui, T. (2006) Numerical simulation of impact cratering on granular material. *Icarus*, *180*, 528–545.
- Walsh, K. J. & Richardson, D. C. (2008) A steady-state model of NEA binaries formed by tidal disruption of gravitational aggregates. *Icarus*, *193*, 553–566.
- Walsh, K. J., Richardson, D. C., & Michel, P. (2008) Rotational breakup as the origin of small binary asteroids. *Nature*, *454*, 188–191.
- Walsh, K. J., Richardson, D. C., & Michel, P. (2012) Spin-up of rubble-pile asteroids: Disruption, satellite formation, and equilibrium shapes. *Icarus*, *220*, 514–529.
- Walton, O. R. & Braun, R. L. (1986) Viscosity, granular-temperature, and stress calculations for shearing assemblies of inelastic, frictional disks. *Journal of Rheology*, *30*, 949.
- Wang, X., Horányi, M., & Robertson, S. (2012) Characteristics of a plasma sheath in a magnetic dipole field: Implications to the solar wind interaction with the lunar magnetic anomalies. *Journal of Geophysical Research: Space Physics*, *117*, A6, n/a–n/a.
- Watters, T. R., Thomas, P. C., & Robinson, M. S. (2011) Thrust faults and the near-surface strength of asteroid 433 Eros. *Geophys. Res. Lett.*, *38*, L02202.
- Williams, D. A., O’Brien, D. P., Schenk, P. M., et al. (2013) Lobate and flow-like features on asteroid vesta. *Planet. Space Sci.*, *0*, –.
- Williams, D. A., Yingst, R. A., & Garry, W. B. (2014) Introduction: The geologic mapping of vesta. *Icarus*, *0*, –.
- Williams, J. (1976) The segregation of particulate materials. A review. *Powder Technology*, *15*, 2, 245 – 251.
- Wilson, L. (2013) Volcanism on differentiated asteroids (Invited). *AGU Fall Meeting Abstracts*, p. A6.
- Wilson, L. & Keil, K. (1996) Volcanic eruptions and intrusions on the asteroid 4 Vesta. *Journal of Geophysical Research*, *101*, 18927–18940.
- Yano, H., Kubota, T., Miyamoto, H., et al. (2006) Touch-down of the Hayabusa spacecraft at the Muses Sea on Itokawa. *Science*, *312*, 5778, 1350–3.
- Yeomans, D. K., Antreasian, P. G., Barriot, J.-P., et al. (2000) Radio Science Results During the NEAR-Shoemaker Spacecraft Rendezvous with Eros. *Science*, *289*, 5487, 2085–2088.
- Yingst, R., Mest, S., Berman, D., et al. (2014) Geologic mapping of vesta. *Planet. Space Sci.*, *0*, –.
- Yu, Y., Richardson, D. C., Michel, P., et al. (2014) Numerical predictions of surface effects during the 2029 close approach of asteroid 99942 apophis. *Icarus*.
- Zuber, M. T., Smith, D. E., Cheng, A. F., et al. (2000) The Shape of 433 Eros from the NEAR-Shoemaker Laser Rangefinder. *Science*, *289*, 5487, 2097–2101.

